Polyester Waste Activated Carbon Assisted Micropollutant Methylene Blue and Congo Red Dyes Removal from Wastewater: RSM Modeling, Kinetics, Mechanism, and Reusability Study

Farhan Raheel Asif[1], Bushra Bibi[1], Muhammad Yasir[2*], Imran Ahmad Khan[3], Jawad Gul[1], Muhammad Irfan[1*], Sofia Javed[1], Vladimir Sedlarik[2]

[1]School of Chemical and Materials Engineering (SCME), National University of Sciences and Technology (NUST), H-12, Islamabad, Pakistan

[2]Centre of Polymer Systems, University Institute, Tomas Bata University in Zlín, Třída Tomáše Bati 5678, 76001 Zlín, Czech Republic

[3]School of Design and Textile, University of Management and Technology, Lahore, Pakistan

***Corresponding authors:** M.Yasir (yasir@utb.cz), M. Irfan (muhammad.irfan@scme.nust.edu.pk)

Abstract

This study explores the synthesis of activated carbon (AC) from polyester waste using zinc chloride ($ZnCl_2$) as a chemical activator, designed to efficiently remove both positive methylene blue (MB) and negatively charged Congo red (CR) dyes from wastewater. Response Surface Methodology integrated with Central Composite Design was employed to optimize critical parameters, including adsorbent dosage, solution pH, dye concentration, and temperature, for enhanced dye removal. The results showed remarkable removal efficiencies of 100% for MB and 99% for CR under optimal conditions. The kinetic analysis showed that the pseudo-second-order model best described the adsorption process because of chemisorption, which includes ion exchange, complexation, π–π stacking, electrostatic interaction, and hydrogen bonding, while intra-particle diffusion was a key factor in the rate-limiting step. The results suggest MB followed the Langmuir isotherm, while the CR adsorption favored both Langmuir and Freundlich models. Thermodynamic studies revealed distinct adsorption behaviors: MB adsorption was exothermic, while CR adsorption was endothermic. Additionally, reusability tests confirmed the material's ability to maintain high performance over five adsorption-desorption cycles with no significant structural changes. These findings underscore the potential of polyester waste-derived AC as a sustainable and effective material for wastewater treatment.

Keywords: Activated carbon, Adsorption, Dye removal, Response Surface Methodology, Wastewater treatment

1. Introduction

Every year, new advancements in polymer technologies are noted. According to recent statistics, the world's polymer production has increased by an average of 37% over the past ten years or almost 100 million metric tons more of polymeric materials. Based on financial analyses, the valuation of the global plastic market in 2020 was approximated at 579.7 billion US dollars, indicating an increase in worth of nearly 15.5% over the preceding five-year period. The global plastic market is expected to reach a value of 750.1 billion US dollars in 2028, growing at a compound yearly growth rate of 3.4% from 2021 to 2028 [1]. However, due to the extended decomposition time of polymeric materials, disposal is a key challenge for polymer-based materials. Consequently, their sustained existence often leads to environmental contamination. Although recycling and repurposing these polymeric wastes to produce secondary materials is the most cost-effective method for their elimination, there has been limited research dedicated to facilitating this process [2]. Glass fiber-reinforced polymers (GFRPs) have emerged as a significant contributor to the growing issue of plastic waste.

Fiber-reinforced polymers (FRPs) have become one of the most widely utilized composite materials in various industries, including automotive, aviation, marine, wind energy, and construction, due to their exceptional specific strength and durability [3]. The annual production of FRPs exceeds 10 million tons, with GFRPs accounting for nearly 90% of the total fiber-reinforced polymer composites (FRPCs) produced each year. The increasing consumption of GFRPs has led to significant waste generation, with over two million metric tons of waste produced annually from end-of-life products and manufacturing processes in the United States alone [4]. The thermosetting polymer matrices, such as polyester, epoxy, and vinyl ester, comprise approximately 70% of the total GFRP production due to their outstanding mechanical properties, high-temperature stability, electrical and corrosion resistance, and low gas permeability [5]. However, the non-biodegradable nature of these composites presents substantial environmental and sustainability challenges during disposal. To address these issues and promote sustainable development in the composite industry, researchers have been exploring various recycling strategies as alternatives to conventional landfill disposal and incineration.

These efforts aim to mitigate the environmental and socio-economic impacts of GFRP waste and contribute to a more circular economy in the composite sector [6].

A forecast indicates that by 2030, the annual demand for accessible freshwater will double from 4500 billion cubic meters a decade ago to 6900 billion cubic meters [7]. Many industries release natural and synthetic dyes into the environment, putting human health and ecosystems at serious risk [8]. Sectors of Textiles, medicines, cosmetics, paper & pulp, leather, plastic, chemical and biological reagents, food, medicine, paint, and dye manufacture are some of these industries [9]. Approximately $2 trillion USD is the global market share of the textile sector, which leads to widespread use and the manufacture of 54% of the organic dye effluents found in the environment globally [10]. According to research, 40 million tons of textiles are produced annually using more than 10,000 tons of dyes in the global economy, which causes 3600 tons of dye waste that is highly concentrated to leak into natural water sources. This is because even minute quantities of contaminants, like dyes, have the potential to disturb the maritime environment directly and adversely affect human and animal health [11]. The wastewater that contains a variety of industrial effluents can have a negative impact on ecological stability. It can also degrade water quality and disrupt photosynthetic processes [12,13].

Methylene blue (3,7-bis(dimethylamino)phenothiazine chloride tetra methylthionine chloride) (MB), a synthetic dye extensively utilized in sectors such as textiles, paper production, food, cosmetics, and pharmaceuticals, presents considerable environmental and health hazards when released untreated into aquatic systems [14]. Human exposure to MB may result in cyanosis, tissue necrosis, emesis, jaundice, and tachycardia, but in plants, it impedes growth and diminishes pigment and protein levels [15]. To alleviate these dangers, regulatory bodies like the Environmental Protection Agency (EPA) impose discharge limitations, recommending a threshold of 0.2 mg/L for MB in wastewater. Compliance with these requirements is essential for safeguarding ecosystems and human health, underscoring the pressing necessity for efficient MB removal methods before the release of industrial effluents [16]. Congo red (1-naphthalene sulfonic acid, 3,3′-(4,4′-biphenylene bis (azo)) bis (4-amino-) disodium salt) (CR), a synthetic anionic azo dye, is extensively utilized in industries like textiles, rubber, plastics, and paper owing to its excellent solubility, durability, and adaptability. It is utilized in histology as a diagnostic agent for amyloidosis and as a pH indicator. Nonetheless, CR is a major

environmental contaminant owing to its bio-recalcitrant characteristics and its toxicity to aquatic organisms [17]. CR presents significant health hazards to humans, including cutaneous and ocular irritation, gastrointestinal discomfort, and dermatitis from acute exposure. Extended exposure is especially perilous, as CR metabolizes into benzidine, a recognized carcinogen associated with cancer [18]. These impacts underscore the imperative for efficient wastewater treatment to avert human exposure and protect health.

The deliberate removal of dyes from water can be accomplished by physicochemical methods such as ion exchange, electrolysis, oxidation, flocculation, and coagulation [19,20]. With less effective color removal, these methods typically show operational and financial drawbacks [21,22]. The alternate method, like adsorption, thereby proves to be successful [23]. The merits of this technique encompass its cost-effectiveness, user-friendly design, resilience against deleterious compounds, and capacity to sequester dye molecules even at minimal concentrations [24]. Activated carbon (AC) is a promising adsorbent for dye adsorption [25]. Adsorption constitutes the mechanism through which dye molecules transition from the film to the carbon surface, approach the boundary layer, and ultimately infiltrate the porous matrix of AC. The exceptional adsorption characteristics of AC are attributed to its complex pore structure and large specific surface area [26,27]. The specific surface area of AC can be significantly augmented through a considerable abundance of microporous configurations, which facilitates the adhesion of adsorption sites [28]. Conversely, mesoporous and macroporous structures contribute to the enhancement of mass transfer efficiency [29]. Carbon, which has substantial hydrophobic qualities, accounts for more than 90% of AC's composition [30]. Furthermore, AC contains oxygen and hydrogen, with oxygen predominantly existing as functional groups like hydroxyl and carboxyl groups that are distributed throughout the AC’s surface [31]. Coal and its processed byproducts are the primary energy source used to produce AC, which involves serious energy consumption and pollution risks [32]. The development of sustainable and environmentally friendly precursor materials for AC production is essential for tackling global energy and ecological issues [33].

The preparation process and the composition of raw materials are crucial in determining the pore structure and performance of AC [34]. Various studies highlight the significance of the activation method, raw material type, and chemical reactions during pyrolysis in shaping the final product's

characteristics. Understanding these factors is essential for optimizing AC production [35]. Using pumpkin peels activated with citric, nitric, and oxalic acids, Jamshaid Rashid et al. synthesized AC has a maximum area of 3.2 m^2/g [36]. Aminu Ibrahim et al. identified a surface area of over 128 m^2/g after treating Melaleuca cajuputi leaves with H_3PO_4 to produce AC [37]. However, this value depends on various factors like the activation method, temperature, and time of activation. This characteristic enhances its effectiveness as an adsorbent for various pollutants, particularly in wastewater treatment applications [38,39]. Common chemical activators include NaOH, KOH, H_3PO_4, $ZnCl_2$, and K_2CO_3 [40]. Among these, $ZnCl_2$ is favored for its efficiency, requiring less energy and producing AC having a more specific surface area [41]. $ZnCl_2$ also serves as a strong dehydrating agent, lowering the decomposition temperature of compounds during activation [42]. Numerous studies have been conducted to investigate the activation mechanism facilitated by $ZnCl_2$. Hu et al. produced activated charcoal through the activation of maize stover lignin using $ZnCl_2$. Through the analysis of a thermogravimetric analyzer (TG) coupled with a Fourier-transform infrared (FTIR) and Pyrolysis–gas chromatography-mass spectrometry (Py-GC/Ms), they observed a significant release of CO_2 and H_2O, which contributed to the formation of pores in the charcoal, thereby elucidating the activation mechanism[43]. Zhihua Xu et al. demonstrate how waste polyester textiles (WPT) can be effectively pyrolyzed and activated to make AC, presenting a beneficial approach for handling textile waste [39]. Additionally, the research highlights the thermal decomposition of WPT in conjunction with $MgCl_2$, which bolsters the efficacy of AC production. Guizhou Huang et al. subjected the WPT to high-temperature pyrolysis with $ZnCl_2$ as an activating agent [44]. This WPT-AC demonstrated an MB removal rate of 97.34%, attributed to mechanisms such as electrostatic attraction and π–π conjugation. Some relevant works include the study of the effect of high pyrolysis temperature on the adsorption performance and the $ZnCl_2$ pre-treatment effect on the number of pores. However, to date, no study has been reported on the area of water treatment using the polyester matrix of waste GFRP, which is an industrial byproduct. Previously Gang Wang et al. showed that it is feasible to create AC with a surface area of 188.7 cm^2/g using waste polyester fabric, suggesting that this source material has great potential [45]. This effort not only addresses waste management but also enhances environmental remediation.

Thus, this study aims to prepare AC from the polyester matrix of GFRP, which has not previously been used as a source for AC, using optimized pyrolysis for the removal of MB (+ve

charged) and CR (-ve charged) dyes. The polyester resin matrix was cured, crushed, and treated with $ZnCl_2$ and then pyrolyzed. The functionalized material was characterized by using Brunauer-Emmett-Teller (BET) analysis, FTIR, X-ray Diffraction (XRD), Energy Dispersive X-ray (EDX), Scanning Electron Microscopy (SEM), and Raman Spectroscopy. Additionally, the Central Composite Design (CCD) model was deployed in combination with response surface methodology (RSM) to enhance the adsorption process, accounting for variables such as temperature, dye concentration, solution pH, and adsorbent dosage. The experimental data was fitted to four kinetic models (Weber-Morris intraparticle diffusion, pseudo-first-order, pseudo-second-order, and the Elovich) and two isothermal models (Langmuir and Freundlich) to understand the interaction mechanism between dyes and AC. Additionally, the impact of temperature on AC's adsorption capacity was examined to demonstrate the thermodynamic behavior. Moreover, fabricated AC was tested for five reusability cycles of each dye, and a mix dye matrix interaction was conducted under optimum conditions.

2. Materials and Methods

2.1. Materials and reagents

The polyester waste was obtained from Fibre Craft Industries (FCI), located in Lahore, Pakistan. All other required chemicals, including MB (>85%), CR (>85%), methylethylketone peroxide (MEKP) (>95%), zinc chloride ($ZnCl_2$) (>98%), and hydrochloric acid (HCl) (37%), were obtained from Sigma Aldrich, Germany.

2.2. Preparation of activated carbon

2.2.1. Step 1: Preparation of Polyester Powder

1% MEKP and 0.5% Cobalt hardener were added to polyester resin and allowed to cure overnight. Once cured, the polyester was crushed using a hammer and then ground into a powdered form. Subsequently, particles larger than 80 mesh were separated using a sieve [46].

2.2.2. Step 2: Pyrolysis of Polyester Powder

The process began by placing polyester powder into a tube furnace under inert conditions, achieved through the introduction of N_2 gas at a flow rate of 80 mL/min. The furnace's temperature was then gradually increased to 500 ℃ @ 10 ℃/min and held constant for 60 min.

The resulting product underwent ball milling for 24 h to refine it into a fine powder, designated as untreated AC (UT-AC).

Concurrently, in a separate series of experiments, the polyester powder underwent mixing with $ZnCl_2$ in a 2:1 ratio ($ZnCl_2$: polyester powder) in 50 mL de-ionized water. This mixture was subjected to continuous stirring overnight at 80 ℃ until it formed a paste. The paste was then introduced into the tube furnace under an inert atmosphere by passing nitrogen gas at a consistent rate of 80 mL/min. The samples were subsequently pyrolyzed at 500 ℃, with the temperature ramped up at a rate of 10 ℃/min and maintained for 60 min. The resultant product was designated as treated AC (T-AC).

The residual carbon was subsequently crushed in a mortar and pestle, followed by washing with 10% HCl and thoroughly rinsing with Deionized water until reaching a pH of 7. The washed carbon was then dried at 100 ℃ in an oven. The resulting powder underwent overnight milling in a ball mill with wet media, followed by drying overnight at 80 ℃, and then the dried powder was stored in a glass veil [47]. The following Schematic diagram (Fig. 1) presents the steps of preparation.

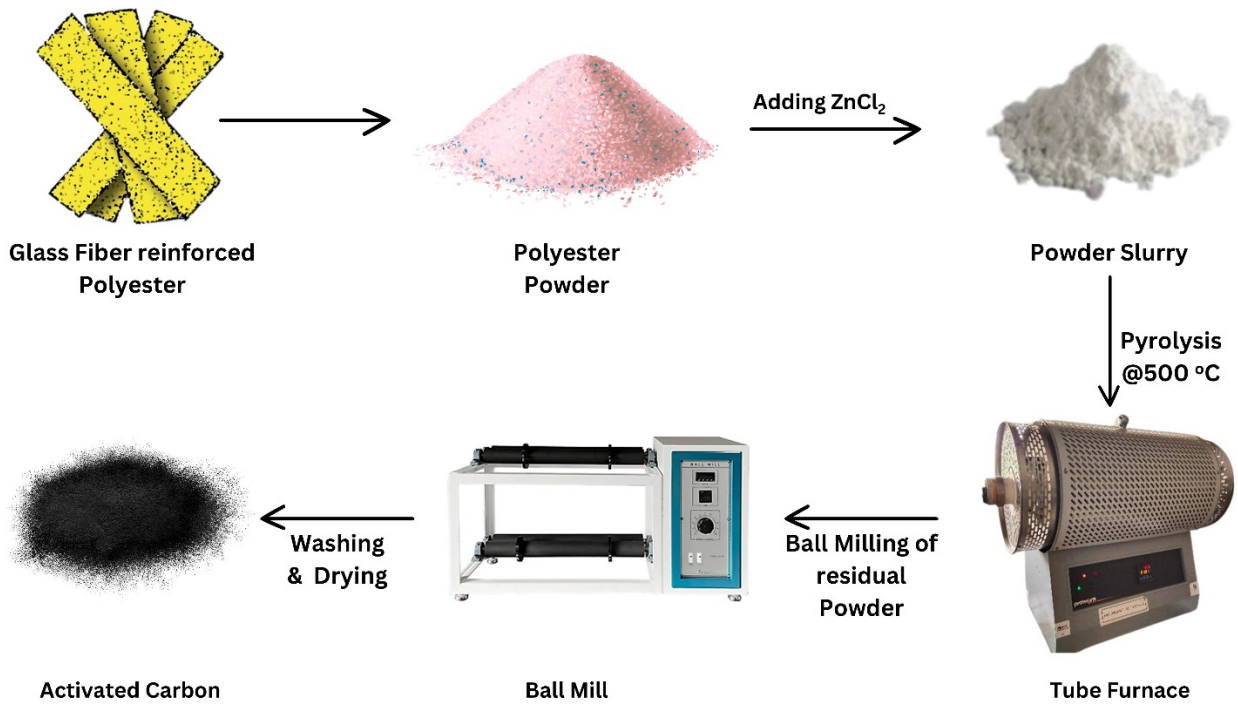

Fig. 1. Schematic Diagram of Methodology for the synthesis of AC by waste GFRP.

2.3. Characterization technique

2.3.1. Fourier-transform infrared spectroscopy (FTIR)

FTIR analysis was carried out using a PerkinElmer Spectrum 100 (USA), designed to detect the functional groups on both treated and untreated ACs using a diamond crystal. Standard settings were used to record spectra with a resolution of 4 cm^{-1}, 64 scans per sample, and a range of 400–4000 cm^{-1}.

2.3.2. Scanning electron microscopy

The surface morphology of the prepared AC was investigated with a JEOL JSM-6490A (Japan) scanning electron microscope (SEM), additionally equipped with Energy Dispersive Spectroscopy (EDX) (JEOL, Japan) for elemental analysis. It was used to investigate the texture, porosity, and general structural properties of the AC. It has a high-resolution capacity of 3.0 nm. The electron beam was operated at an accelerating voltage appropriate for detailed surface imaging, which guaranteed clear feature visualization.

2.3.3. X-ray Diffraction (XRD)

The AC produced was subjected to X-ray diffraction (XRD) analysis using a D2 Phasor diffractometer (Bruker, Rotterdam, Netherlands). The measurements were taken using a scanning rate of 2 °/min over a 2θ range of 10–90°. In order to comprehend the AC's adsorption behavior and structural integrity, this arrangement offered comprehensive insights into its crystalline structure and phase composition.

2.3.4. Raman Spectroscopy

The obtained AC's degree of graphitization and defect morphology were examined by Raman spectroscopy utilizing a Raman Technique BWS415-532S-iRaman (Newark, NJ, USA). Plotting Raman shift versus intensity graphs was used in the research to determine the distinctive D band, which is linked to structural flaws, and the G band, which is suggestive of graphitic structures.

2.3.5. UV-Visible Spectroscopy

The concentrations of MB and CR in the solutions were assessed utilizing a Jenway™ Model 7315 UV/Visible Single Beam Spectrophotometer (Fisher Scientific Inc., USA.) at wavelengths of 665 nm and 498 nm, respectively [48].

2.3.6. BET- Brunauer–Emmett–Teller

The characterization of the obtained ACs was conducted through N_2 adsorption at −196 °C using a surface area and pore size analyzer (model TriStar II 3020, Micromeritics, USA). Prior to analysis, all ACs were subjected to overnight evacuation under vacuum conditions at 150 °C to cleanse the pores thoroughly. The Brunauer–Emmett–Teller (BET) equation was used to calculate the BET surface area from the isotherms.

2.3.7. Zeta potential

The point of zero charge (pH_{ZPC}) is the pH at which an adsorbent surface becomes electrically neutral, serving as a key parameter for assessing electrostatic interactions between the adsorbent and adsorbate. To analyze this property, the zeta potential of T-AC was determined at pH 2, 7, and 11 using a Zetasizer (Malvern Instruments Inc., UK), offering valuable insights into surface charge behavior across different pH levels.

2.4. Adsorption experimental design

2.4.1. Preparation of Dye Solutions

A 1000 mg/L stock solution of MB and CR was developed by dissolving 1g of each dye in 1 liter of deionized water separately. From this stock solution, dilutions were made to obtain solutions of 1, 5, 25, 35, 45, and 49 mg/L concentrations for calibration. Each experiment utilized 20 mL of the respective dye solution [49]. The characteristics of each dye are presented in Table 1.

Table 1. Chemical structures of dyes used in this study [49].

Dye	Structure	Charge	Molar Weight (g/mol)	λ_{max} (nm)

MB	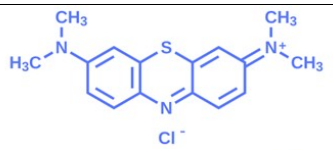	+1	319.85	665
CR	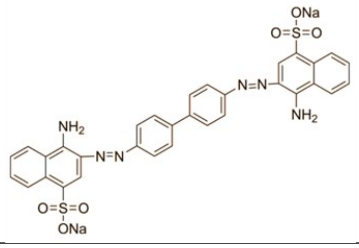	-1	696.65	498

2.4.2. *Batch adsorption testing*

Batch static adsorption studies were carried out to ascertain the produced AC's removal capability and efficiency. A 20 mL dye solution was used to evaluate adsorption efficiency. The flasks were continuously agitated using a Digital Thermostat Incubator with Shaker (Wincom Inc., China) at 130 rpm while varying different parameters, including the initial dye concentration (mg/L), solution pH, adsorbent dosage (mg), and the temperature of the dye solution (℃). The study further computed the dyes' equilibrium adsorption capacity and removal percentages using mathematical Eq. (1) and (2), respectively.

$$Dye\ uptake\left(q_e\right)=v\times\frac{\left(C_i-C_e\right)}{M}\left(1\right)$$

$$Dye\ removal\left(\%\right)=\frac{C_i-C_t}{C_i}\times 100\left(2\right)$$

where C_i is the initial concentration (mg/L), and C_t is the concentration of the solution at time t (mg/L). M is the mass of adsorbent (g), V is the volume of solution (L), and q_e is equal to the equilibrium adsorption capacity (mg/g).

The most important parameters and their combined impacts on the removal of MB and CR dye by the produced AC were estimated and optimized using the Central Composite Design (CCD) model and Design-Expert software v13.0. The axial and central points are represented by the factorial points that make up CCD. The levels of the main factors investigated are given in Table 2. In order to model the dyes' responses, a second-order polynomial equation is fitted to the

relationship between these independent components depending on the response received, which is expressed by Eq. (3).

$$Y = \beta_o + \sum_{i=1}^{k} \beta_i X_i + \sum_{i=1}^{k} \beta_{ii} X_i^2 + \sum_{i=1}^{k} \sum_{j=i+1}^{k} \beta_{ij} X_i X_j + \varepsilon \quad (3)$$

Here, Y represents the response (removal efficiency), while X_i and X_{ij} denote the encoded parameters. The coefficients β_0, β_i, $\beta_{ii,}$ and β_{ij} correspond to the linear, quadratic, and interaction terms, respectively. The desirability function is applied to the results obtained to optimize the parameters investigated, determining the optimal levels for each factor.

Table 2. Experimental factors and their corresponding levels analyzed in the CCD model.

Factors	**Low(-1)**	**Center (0)**	**High (+1)**
A – Temperature (^oC)	25.00	35.00	45.00
B – Solution pH	3.00	7.00	11.00
C – Initial conc. of Dyes (mg/L)	5	25	45
D – Adsorbent dosage (mg)	10.00	30.00	50.00

2.5. Adsorption Kinetics

The adsorption kinetics of MB and CR dyes onto activated carbon were investigated in order to determine the rate-limiting phase and investigate the factors influencing the adsorption process, such as mass transfer mechanisms and chemical interactions. The adsorption behavior was investigated using four well-known kinetic models: Weber-Morris intra-particle diffusion, pseudo-first-order, pseudo-second-order, and Elovich. These models improved the process parameters for effective dye removal and offered insightful information about the adsorption mechanisms [50].

The difference between the quantity adsorbed at equilibrium and the rate of dye adsorption is precisely proportional to the amount adsorbed at any given moment, according to Lagergren's pseudo-first-order model. It is given as follows:

$$\log(q_e - q_t) = \log q_e - \frac{K_1}{2.303} t \quad (4)$$

Where k_1 (L/min) is the first-order rate constant, q_t (mg/g) is the quantity of dye adsorbed at time t, and q_e (mg/g) is the quantity adsorbed at equilibrium. Early on in the adsorption process, the model fit MB and CR well, indicating that physisorption predominated. Its failure to adequately characterize the long-term adsorption, however, suggested the presence of more intricate interactions. The pseudo-second-order model, on the other hand, more accurately depicted the adsorption process for both MB and CR because it is assumed that the rate-limiting stage in which dye molecules and activated carbon surface active sites interact significantly is chemisorption. This model can be written as:

$$\frac{t}{q_t}=\frac{1}{K_2 q_e^2}+\frac{t}{q_e} \quad (5)$$

where the second-order rate constant is denoted by k_2 (g/(mg·min)). This model's strong agreement with experimental data indicates that chemical bonding was crucial to both dyes' adsorption.

The Weber-Morris intra-particle diffusion model was used to evaluate the role of diffusion mechanisms. According to this concept, the process of adsorption involves several steps, including the transport of dye molecules from the bulk solution to the surface of the adsorbent and their diffusion via the pores. It is as follows:

$$q_t=K_3 t^{0.5}+C \quad (6)$$

Where C (mg/g) is the thickness of the boundary layer, and k_3 (mg/g·h$^{1/2}$) is the intra-particle diffusion rate constant. The Weber-Morris plots' linearity suggested that intra-particle diffusion had a role in the adsorption process. The departure from the origin, however, implied that external mass transfer and surface adsorption were also important. The Elovich model was found to be most suitable for interactions where chemisorption predominates. It explains the adsorption process in which the rate gradually drops as a result of the active sites gradually becoming covered. The model is stated as follows:

$$q_t=\beta \ln(\alpha\beta)+\beta \ln(t) \quad (7)$$

Where the desorption constant is β (mg/g), and the initial adsorption rate is α (mg/g·min). The gradual drop in MB and CR's adsorption rates suggested that the process was dominated by chemisorption, with dye molecules and the activated carbon surface developing irreversible connections [51].

2.6. Isotherm Modeling

The adsorption behavior of the AC samples was examined using the Langmuir and Freundlich models, as described by Eq. (8) and (9), respectively.

$$\frac{1}{q_e}=\frac{1}{K_L.q_{max}}.\frac{1}{C_e}+\frac{1}{q_{max}} \quad (8)$$

Here, q_{max} (mg/g) represents the highest adsorption capacity that monolayer coverage corresponds to, K_L (L/mg) denotes the Langmuir adsorption constant, and C_e is the experimentally measured concentration of the adsorbed contaminant.

$$\log q_e=\log K_f+\frac{1}{n}.\log C_e \quad (9)$$

K_f represents the Freundlich adsorption constant, while *1/n* denotes the heterogeneity factor associated with the adsorption process.

2.7. Thermodynamic Study

In a temperature-controlled system, the impact of temperature on activated carbon's adsorption capability was examined at 23 ℃, 35 ℃, and 47 ℃. The adsorption process's thermodynamics was assessed using the following formulas: [52,53]

$$K_D=\frac{C_s}{C_e} \quad (10)$$

$$lnK_D=\frac{-\Delta H}{RT}+\frac{\Delta S}{R} \quad (11)$$

$$\Delta G=\Delta H-T\,\Delta S \quad (12)$$

Here, ΔG represents the Gibbs free energy change, ΔH is the enthalpy change, and ΔS is the entropy change. K_D is the distribution coefficient (the ratio of the adsorbate concentration on the solid phase to that in the solution), R (8.314 J/mol·K) is the universal gas constant, C_s (mg/L) is

the concentration of the adsorbate on the activated carbon, and T (K) is the absolute temperature. By plotting a Van't Hoff plot of lnK_D versus $1/T$, ΔS, and ΔH were determined from the slope and intercept, respectively. Values of ΔG at different temperatures were then calculated and are given in Table 9.

2.8. Adsorption-desorption analysis and reusability

In the reusability test, 30 mg of treated activated carbon (AC) was added to 20 mL of dye solution, with pH 12 for MB and pH 7 for CR. The mixtures were incubated at 35 ℃ and gently shaken at 130 rpm using an automatic shaker for 2 h to facilitate adsorption. After adsorption, samples were taken for measurement, and the remaining solvent was evaporated through heating. The residual powder was placed in an oven overnight and reused in the next adsorption cycle. All measurements were made in triplicate, and average values were noted for the five successive adsorption-desorption cycles in which this process was repeated.

2.9. Statistical and error analysis

The data are presented as Mean ± Standard Error. Statistical analysis was conducted using OriginLab 2024b and Design Expert software v.13.0. Differences between values were assessed through one-way analysis of variance (ANOVA), with statistical significance set at $p < 0.05$. To evaluate the accuracy of the experimental and theoretical data, error analysis parameters such as the determination coefficient (R^2) were utilized. Additionally, error minimization was performed using the sum of squared errors (SSE) test to address biases inherent in the linearization of equations, particularly in kinetic modeling.

3. Results and discussion

3.1. Material characterization

3.1.1. Scanning Electron Microscope

The morphology of UT-AC was observed to have a regular structure, as shown in Fig. 2 (a & b). The size of the regular-shaped planes ranged from 2 to 8 μm. The additive $ZnCl_2$ altered the regular surface of AC, and bulk carbon transformed into a loose, irregular, rough surface. Course surface with heterogenous fluffy, highly porous adsorbent surface. Furthermore, according to the results of EDX analysis, T-AC contained carbon (82.7 %), oxygen (14.7 %), Magnesium (2.0

%), fluorine (0.5 %), and silicon (0.1 %). Bearing rough microstructure, the overall morphology of T-AC is in agreement with the remediation of MB dye due to fertile preconditions and morphological cracks, as shown in Fig 2 (c & d). Xiaoying Yu et al. used Polyester fabric to produce AC to remove MB and have reported similar results. [38,54]. These findings were further supported by BET analysis, which showed a substantial increase in the number of accessible adsorption sites with a BET surface area of 167.08 m^2/g and a Langmuir surface area of 243.35 m^2/g. With a micropore volume of 0.0214 cm^3/g, micropores made up 53.23 m^2/g of the surface area. Additionally, the material has pore diameters up to 27.34 Å and a large exterior surface area of 113.84 m^2/g. These features highlight T-AC's improved adsorption capacity, which makes it ideal for dye remediation in aqueous solutions.

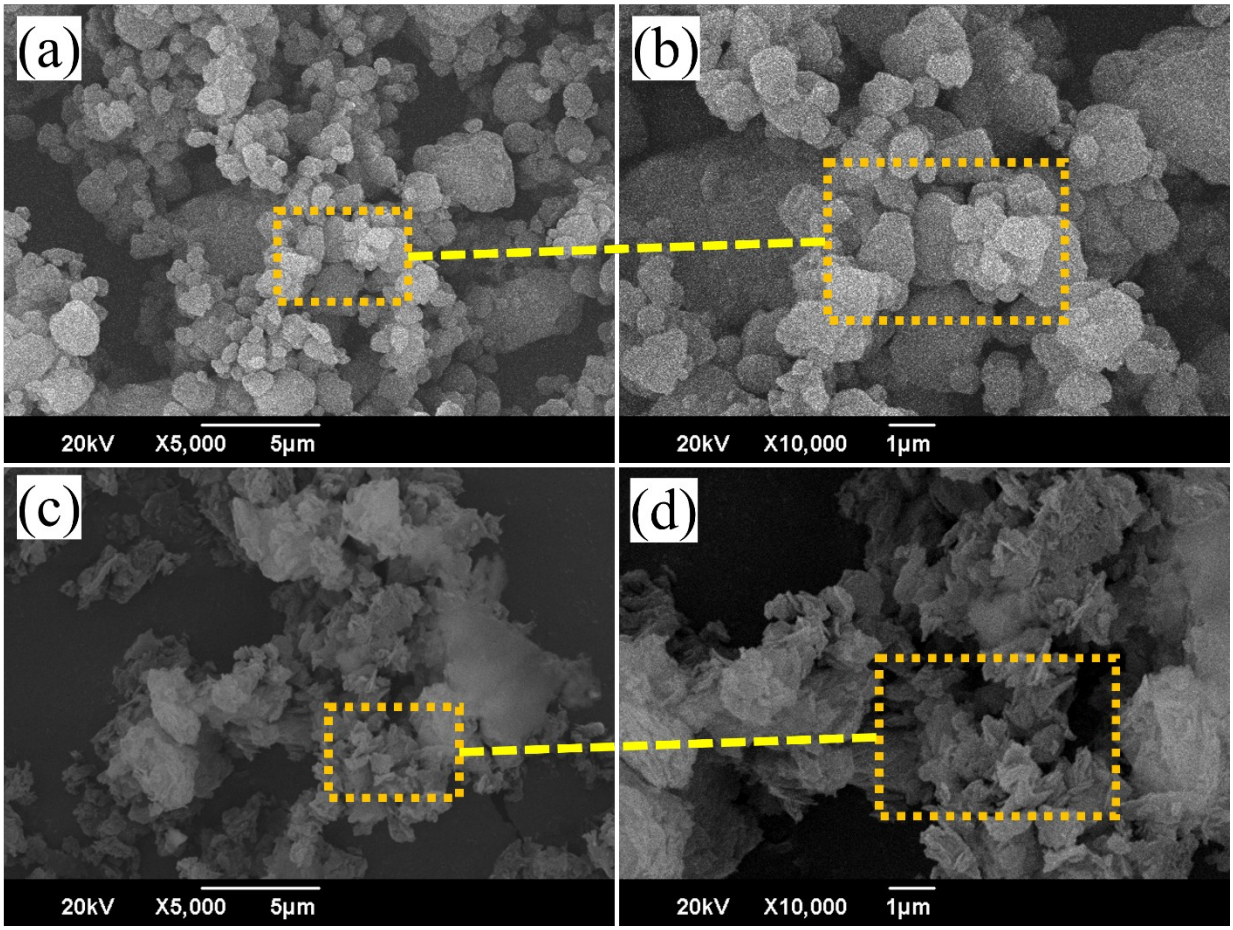

Fig. 2. SEM images of UT-AC (a & b) and T-AC (c & d).

3.1.2. *Fourier Transform Infrared Spectroscopy*

The functional groups of treated and untreated AC reveal significant capability for the adsorption of MB. A wide band between 3000-3600 cm^{-1} normally confirms the presence of the O-H group. The broad peak between 3000-3500 cm^{-1} in both samples corresponds to O-H stretching, as shown in Fig. 3(a), indicating the presence of hydroxyl groups, which can enhance hydrogen bonding with MB [55]. The symmetric and the asymmetric vibrations of C-H are observed at 2900 cm^{-1} [56]. The more intense peak around 1700 cm^{-1} in T-AC suggests an increase in C=O stretching, likely from carbonyl groups, which promote electrostatic interactions with MB. Aromatic C=C stretching bands near 1500-1600 cm^{-1} in both spectra indicate the presence of aromatic rings, essential for π-π stacking with MB's aromatic structure. Peaks between 1000-1300 cm^{-1}, sharper in T-AC, correspond to C-O stretching, which contributes additional polarity and may improve dye adsorption. Overall, T-AC has more oxygenated functional groups, such as carbonyl and ether, enhancing its capacity for MB removal through stronger electrostatic interactions and surface polarity compared to UT-AC.

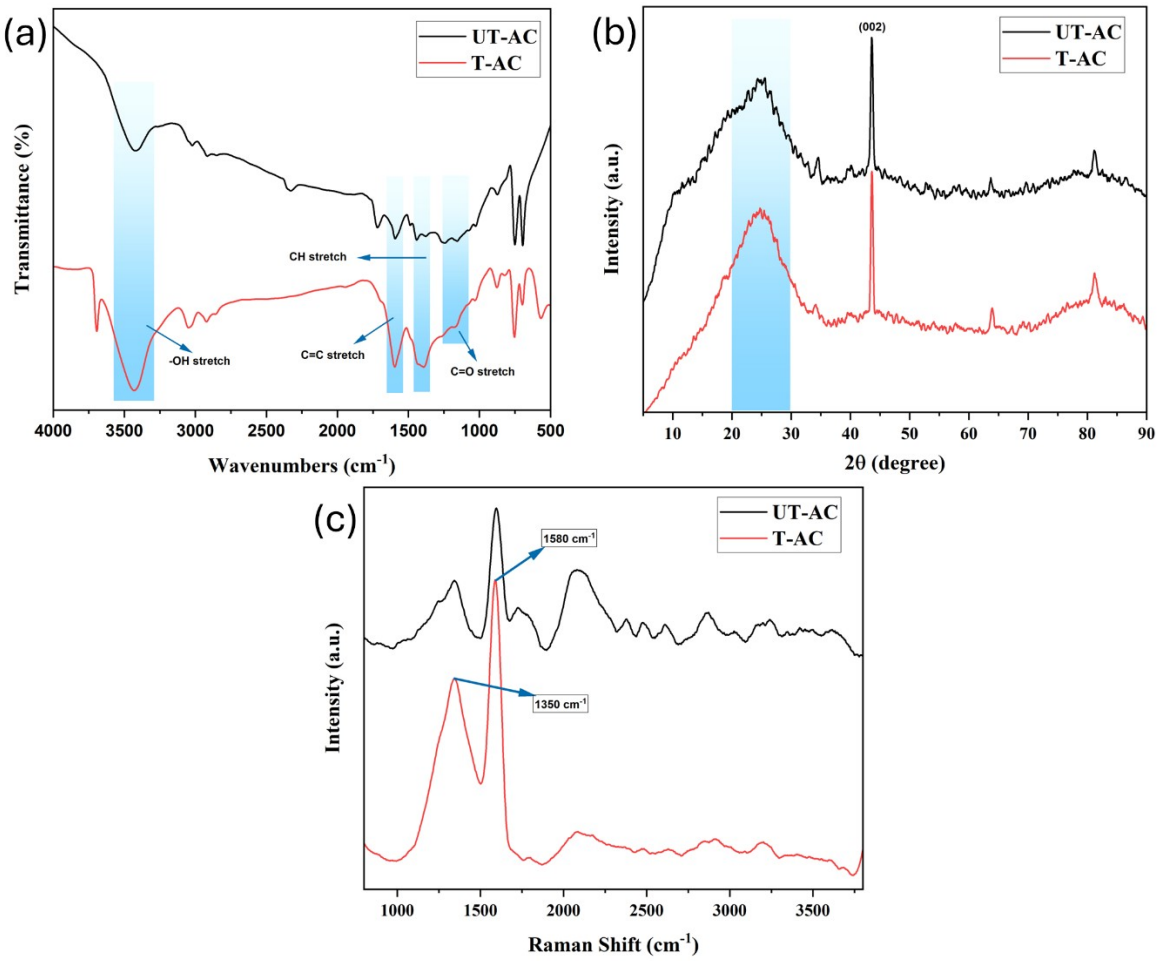

Fig. 3. (a) FTIR Spectroscopy, (b) XRD, and (c) Raman Spectroscopy of treated and untreated AC.

3.1.3. X-Ray Diffraction

The XRD patterns of T-AC and UT-AC primarily reflect the presence of amorphous carbon, as evident from the broad peak between 2θ = 20-30°. The peak intensity differences suggest that the treatment process has affected the carbon structure, possibly due to changes in surface functional groups or defects rather than graphitic ordering. The distinct peak around 2θ = 43-45° could instead correspond to the stub material or other non-graphitic carbon-related structures introduced during the preparation process. In T-AC, this peak is diminished, implying that the treatment has disrupted the graphitic structure, resulting in a more amorphous form. The reduction in graphitic content and increase in amorphous character in T-AC likely enhance its adsorption properties, as the disordered structure provides a greater surface area and more active

sites for adsorption. Additionally, the increase in surface defects in T-AC, caused by the disruption of crystallinity, may further contribute to its improved capacity for dye removal [57].

3.1.4. Raman Spectroscopy

The Raman spectra of T-AC and UT-AC reveal differences in structural disorder that are crucial for MB adsorption. Both samples exhibit two key peaks: the D-band near 1350 cm^{-1}, associated with structural defects, and the G-band around 1580 cm^{-1}, linked to graphitic carbon with sp^2 hybridization, as shown in Fig. 3(c) [58]. In UT-AC, the G-band is more prominent, reflecting a higher degree of graphitic order and fewer defects. In contrast, T-AC shows a significantly stronger D-band relative to the G-band, indicating an increase in structural defects after treatment. The higher intensity ratio of the D-band to the G-band (I_D/I_G) in T-AC suggests a greater degree of disorder, which enhances the availability of active sites for dye adsorption. This increased defect density in T-AC facilitates stronger interactions with the dye molecules, improving its adsorption capacity. Consequently, the treatment process enhances the surface reactivity of T-AC, making it more effective for MB and CR removal compared to the more graphetically ordered UT-AC.

3.2. Batch adsorption optimization study

Analyzing the experimental data allowed for the determination of the ideal adsorption parametric settings for this investigation, which was obtained (Table 3) through the response surface methodology in the CCD model.

3.2.1. ANOVA for quadratic model of MB

This study employed Design-Expert Software version 13 (DX 10) for statistical analysis. An analysis of variance (ANOVA) was carried out to evaluate the variation among the experimental factors, comprising Dye concentration (A), pH (B), AC concentration (C), and temperature (D), and their influence on MB removal. Table 3 displays the input parameters and associated responses for MB removal. To determine the connection between the response in terms of MB removal and the input parameters, an equation was devised, as illustrated by Eq. (13).

$$MB\,removal\ percentage = 93.8 - 2.95\,A + 20.28\,B + 20.55\,C - 0.55\,D + 3.87\,AB + 3.39\,AC + 0.59\,AD - 20.33\,BC + 0.7 \quad (13)$$

Table 3. Regression analysis of MB removal via ANOVA modeling.

Run	Dye Conc.	pH	Ac Dosage (mg)	Temperature (°C)	MB removal percentage	MB removal predicted
1	5	11	50	25	99.9877	93.91
2	45	11	50	45	99.962	104.13
3	45	3	10	25	2.35592	7.9
4	5	3	50	25	99.6837	103.29
5	5	3	10	25	36.1445	29.49
6	25	7	6	35	52.7369	55.01
7	45	3	50	45	97.3632	94.95
8	5	3	50	45	99.5744	100.63
9	45	3	10	45	1.64155	5.24
10	25	7	30	35	99.4654	93.83
11	25	7	30	35	99.4654	93.83
12	1	7	30	35	79.4777	89.22
13	5	3	10	45	25.7118	24.46
14	5	11	50	45	99.7797	94.34
15	49	7	30	35	85.276	82.14
16	25	7	30	23	99.8383	103.77
17	25	7	30	35	99.4654	93.83
18	5	11	10	45	99.7299	99.49
19	45	11	10	25	98.8534	95.31
20	25	2.2	30	35	61.334	59.63
21	45	11	50	25	99.9813	101.34
22	25	7	54	35	99.9982	104.33
23	45	3	50	25	97.4931	95.25
24	25	11.8	30	35	99.9931	108.3
25	25	7	30	47	99.7456	102.43
26	5	11	10	25	98.9103	101.43
27	45	11	10	45	99.2298	95.73

Regression analysis was utilized to calculate the correlation coefficient (R^2) and assess the variability and accuracy of the developed models as per Table 4. The Model F-value of 38.28 implies the model is significant. There is only a 0.01% chance that an F-value this large could occur due to noise. P-values less than 0.0500 indicate model terms are significant. In this case, B, C, AB, BC, B^2, and C^2 are significant model terms. Values greater than 0.1000 indicate the model terms are not significant. The R^2 value of 0.979, nearing 1, demonstrates the model's validity.

436 **Table 4.** ANOVA analysis, assessing the impact of input variables (factors) on the percentage of
437 MB removal (response).

Source	Sum of Squares	df	Mean Square	F-value	p-value	R^2
Model	24568.94	14	1754.92	38.28	< 0.0001	0.979
A-Dye Conc.	164.23	1	164.23	3.58	0.0827	
B-pH	7763.74	1	7763.74	169.37	< 0.0001	
C-AC dosage	7972.14	1	7972.14	173.92	< 0.0001	
D-Temperature	5.87	1	5.87	0.1281	0.7266	
AB	239.32	1	239.32	5.22	0.0413	
AC	183.53	1	183.53	4	0.0685	
AD	5.57	1	5.57	0.1216	0.7334	
BC	6612.67	1	6612.67	144.26	< 0.0001	
BD	9.54	1	9.54	0.2081	0.6564	
CD	5.62	1	5.62	0.1227	0.7322	
A^2	162.31	1	162.31	3.54	0.0843	
B^2	237.77	1	237.77	5.19	0.0419	
C^2	490.14	1	490.14	10.69	0.0067	
D^2	210.18	1	210.18	4.59	0.0535	
Residual	550.06	12	45.84			
Lack of Fit	550.06	10	55.01			
Pure Error	0	2	0			

438

Figure 4a illustrates the impact of MB concentration and pH on adsorption effectiveness. It's evident that higher pH values and lower dye concentrations favor removal efficiency. Specifically, removal efficiency increases from 68% to 100% as pH rises from 3 to 11, with a constant MB concentration of 5 mg/L. The optimum dye concentration is observed at 25 mg/L and a pH of 11, resulting in a removal efficiency of 100%. This is in contrast to a dye concentration of 45 mg/L and a pH of 3, where the removal efficiency is found to be 54%. At initial pH levels below 5, the adsorption efficiency of MB dye using the prepared adsorbent is minimal, suggesting that acidic pH conditions are unsuitable for the adsorption of MB dye. This can be explained based on the cationic properties of MB dye, as at acidic pH levels, the adsorbent's surface carries a positive charge. Consequently, the positively charged MB cationic dye is repelled by the positively charged adsorbent surface. So, these results may be correlated to the generation of an attractive electrostatic force between the adsorbent surface and dye molecules in basic solution conditions and, conversely, a repulsive electrostatic force in acidic conditions [59]. Therefore, high pH values lead to higher removal efficiency.

A similar trend is noted for the AC dosage, as depicted in Figure 4b, wherein the removal percentage rises from 64% to 98% with an increase in AC dosage from 10 mg to 50 mg. In contrast, the removal efficiency of the prepared AC dropped to just 50% when the concentration of dye was raised to 45 mg/L by using the 10 mg of AC dosage. In this case, the optimum dye concentration is observed at 25 mg/L and AC dosage of 50 mg, resulting in a removal efficiency of 100%. This can be explained by increasing the adsorbent dosage at a constant pollutant concentration, which appears to enhance the availability of active surfaces for adsorption. Thus, the low removal percentages are attributed to the limited quantity of the AC powdered sample available for interaction with higher concentrations of dye molecules [60]. The graph depicted in Figure 4b also indicates a decrease in the adsorption (%) of MB from 64% to 53% when the starting dye concentration rose from 5 to 45 mg/L. This decline in the efficiency of dye removal can be attributed to the lack of accessible active sites under high MB concentration conditions, leading to a decrease in the extent of dye removal [61].

The impact of temperature vs. MB concentration on MB removal is shown in Figure 4c. The removal of dye showed a slight increase of 6% within the range of 35 to 45 ℃. Overall, the removal is over 80% for all values of concentration (5 to 45 mg/L) variation with temperature

changing from 25 to 45 ℃. However, at low concentrations, the removal of MB is higher compared to high concentrations, regardless of change in temperature. This could be due to the sufficient availability of sites at low MB concentrations while all adsorption sites are occupied at high MB concentrations, and the solution remains in excess.

The most significant impact on the removal percentage is evident in Figure 4d, where lower pH and lower AC dosage result in just 17% MB removal percentage, changing abruptly with the high pH 11 and AC dose (50 mg) combination, which achieves 98% dye removal percentage. As previously discussed, the adsorption of MB was found to be directly correlated with pH and the dosage of AC. On the contrary, at lower pH levels (3) and AC dosages (10), the lowest removal of MB was observed, amounting to 16%. Conversely, the highest removal of MB (98%) was achieved with higher pH levels (11) and AC dosages (50), attributed to their synergistic effect.

The influence of temperature with pH on MB removal is depicted in Figure 4e. As can be seen at elevated pH and temperature levels, nearly 100% removal of MB was achieved, primarily attributed to the synergistic effect. The nature of a process can be understood by observing how it responds to changes in temperature. An endothermic process or reaction experiences an increase in dye sorption on the adsorbent with rising temperature, whereas an exothermic process sees a decrease in adsorption capacity as temperature increases. However, the effect of pH on removal is more dominant; at low temperatures and pH, only 74% of the removal was observed. Moreover, At a low pH of 3, the rise in the temperature from 25 to 45 ℃ has a negligible contribution to MB removal (experiments 7 and 23), indicating exothermic behavior. Whereas at a high pH of 11, MB dye adsorption exhibits endothermic behavior with a rise in MB removal from 98.9 to 99.7 % at a concentration of 5 mg/L when the temperature was raised from 25 to 45 ℃. Another study reported similar behavior of MB removal [62].

The effect of AC dosage and solution temperature on MB removal is depicted in Figure 4f. As can be seen, when both temperature and dosage are low, the removal of MB is at 71%. However, as the temperature rises to 45 ℃ and the dosage of AC reaches 50 mg, the removal of MB increases to 100%, indicating this as one of the optimal conditions for achieving peak removal performance. This is primarily attributed to two main effects of temperature: First, the pace at

497 which dye molecules diffuse across AC's exterior increases; second, there is a greater mobility of
498 molecules, which lowers viscosity [63,64].

499

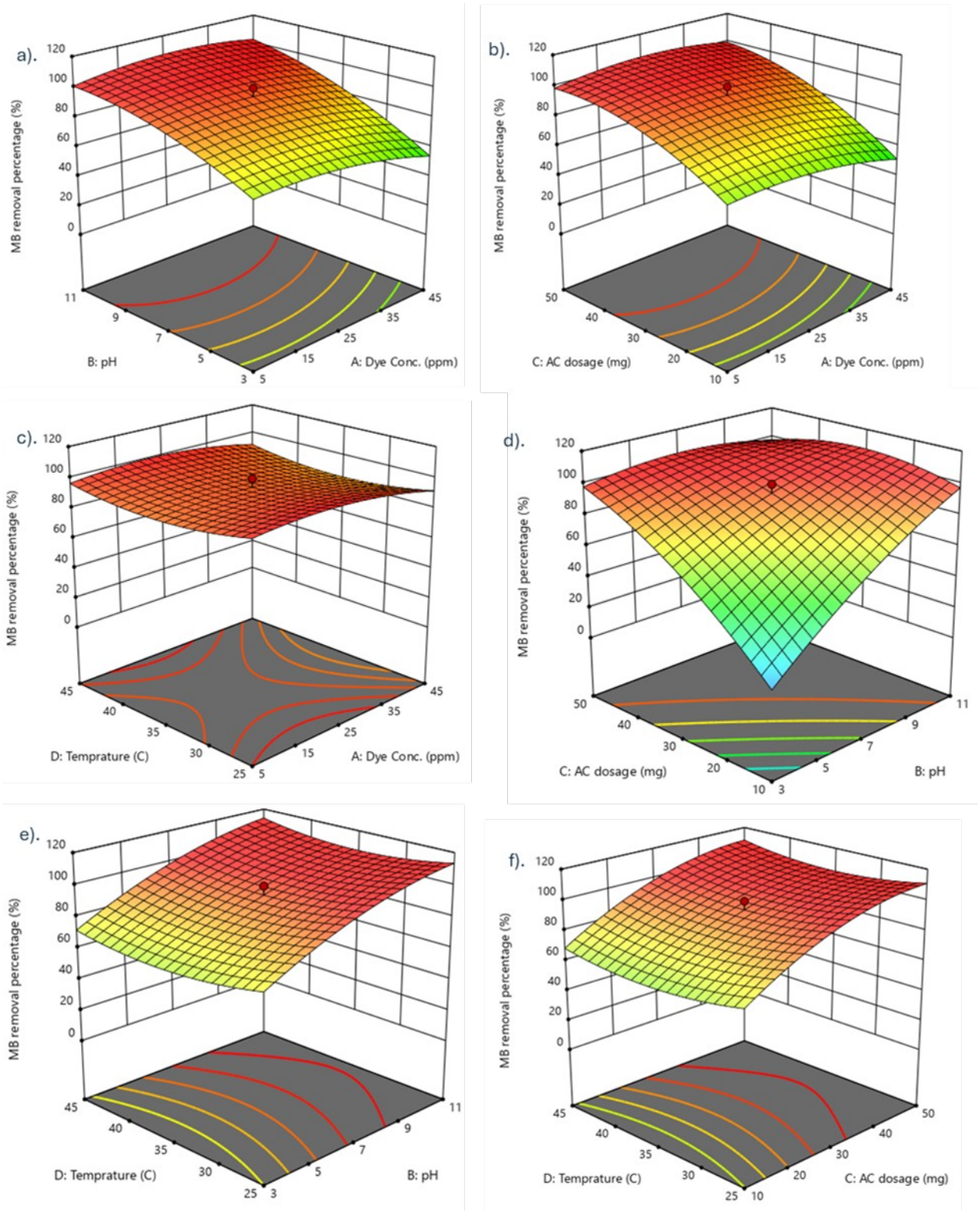

Fig. 4. 3D response surface plot for MB removal as a function of (a) pH versus dye concentration, (b) AC dose versus dye concentration, and (c) Temperature versus dye concentration. (d) AC versus pH (e) Temperature versus pH (f) Temperature versus AC dose.

3.2.2. ANOVA for quadratic model of CR

Table 5 displays the input parameters and associated responses for CR removal. An equation was formulated with the intent of defining the relation between the input variables and the corresponding outcome regarding CR removal, as depicted in Eq. (14).

$$CR\,removal\,percentage = 101.3 + 5.82\,A - 1.76\,B - 0.70\,C - 2.49\,D + 1.36\,AB + 1.35\,AC + 3.05\,AD + 1.9\,BC - 1.05\,BI \quad (14)$$

Table 5. Regression analysis of CR removal via ANOVA modeling.

Run	Dye Conc.	pH	Ac Dosage (mg)	Temperature (°C)	CR removal percentage	CR removal percentage (Predicted)
1	5	11	50	25	90.5588	89.87
2	45	11	50	45	97.1025	97.49
3	45	3	10	25	99.0295	95.89
4	5	3	50	25	91.8413	90.2
5	5	3	10	25	92.2592	95.76
6	25	7	6	35	99.1005	99.22
7	45	3	50	45	99.1879	96.6
8	5	3	50	45	73.032	78.88
9	45	3	10	45	96.887	101.46
10	25	7	30	35	99.765	101.36
11	25	7	30	35	99.765	101.36
12	1	7	30	35	92.8718	88.37
13	5	3	10	45	95.2574	89.13
14	5	11	50	45	74.4191	74.34
15	49	7	30	35	99.7012	102.34
16	25	7	30	23	98.2174	101.06
17	25	7	30	35	99.765	101.36
18	5	11	10	45	71.5403	76.98
19	45	11	10	25	95.3426	93.38
20	25	2.2	30	35	99.9957	101.1
21	45	11	50	25	97.9054	100.81
22	25	7	54	35	99.5083	97.53
23	45	3	50	25	97.2629	95.72
24	25	11.8	30	35	99.8418	96.87
25	25	7	30	47	99.7906	95.08
26	5	11	10	25	88.4495	87.82
27	45	11	10	45	96.3201	94.74

Regression analysis was utilized to calculate the correlation coefficient (R^2) and assess the variability and accuracy of the developed models as per Table 6. The significance of the model is indicated by its F-value of 5.26. The likelihood that an F-value this large may be caused by noise is merely 0.33%. Model terms are considered significant when the P-value is less than 0.0500. A, D, and AD are significant model terms in this instance. The model terms are not significant if the values are higher than 0.1000. The model's validity is reasonably supported by the R^2 of 0.860.

Table 6. ANOVA analysis, assessing the impact of input variables (factors) on the percentage of CR removal (response).

Source	Sum of Squares	df	Mean Square	F-value	p-value	R^2
Model	1541.24	14	110.09	5.26	0.0033	0.860
A-Dye Conc.	639.44	1	639.44	30.57	0.0001	
B-pH	58.75	1	58.75	2.81	0.1196	
C-AC dosage	9.35	1	9.35	0.447	0.5164	
D-Temperature	117.08	1	117.08	5.6	0.0357	
AB	29.5	1	29.5	1.41	0.258	
AC	28.98	1	28.98	1.39	0.262	
AD	148.94	1	148.94	7.12	0.0205	
BC	57.92	1	57.92	2.77	0.122	
BD	17.74	1	17.74	0.8479	0.3753	

CD	21.97	1	21.97	1.05	0.3256
A^2	88.08	1	88.08	4.21	0.0626
B^2	13.72	1	13.72	0.6559	0.4338
C^2	21.76	1	21.76	1.04	0.3279
D^2	26.37	1	26.37	1.26	0.2835
Residual	251.01	12	20.92		
Lack of Fit	251.01	10	25.1		
Pure Error	0	2	0		

Figure 5a demonstrates how both pH and the initial concentration of CR influence the efficiency of adsorption. The pH is essential for regulating a number of variables, such as the adsorbent's surface charge, the degree of adsorbate ionization in the solution, and the dissociation of different functional groups on the adsorbent's active sites [65]. It's clear from the data that higher pH levels lead to a decrease in CR removal efficiency. Specifically, the efficiency of removal decreases from 92% to 86% as the pH increases from 3 to 11 while maintaining a constant CR concentration of 5 mg/L. This may be due to the creation of repulsive electrostatic forces between the adsorbent surface and dye molecules in basic solution conditions, while attractive electrostatic forces occur in acidic conditions [66]. CR is an amphoteric molecule and exhibits zwitterionic behavior depending on the pH of the solution. At higher pH, CR may exist in its anionic form, reducing the strength of electrostatic interactions with the negatively charged T-AC surface (deprotonated $-O^-$ groups). This weakens adsorption efficiency despite the presence of Na^+ ions [67]. On the contrary, the quantity of CR adsorbed increased with higher dye concentrations. The findings indicated that higher initial dye concentrations resulted in increased adsorption. Apparently, the initial dye concentration significantly influences its adsorption capacity. A higher concentration of CR enhances the driving forces of the concentration gradient, thereby increasing the adsorption capacity [63].

For the dosage of AC, as shown in Figure 5b, the removal percentage increased from 90% to 92% with an increase in AC dosage from 10 mg to 30 mg. The amount of dye adsorbed, however, decreased as the dosage increased to 50 mg. This may have happened because the active sites overlapping or aggregating as the dosage rose made the sites inaccessible to the dye [68]. The combined effect of the AC dose in the range of 20 mg to 30 mg and high dye concentration (45 mg/L) results in the removal of almost 100% dyes from the solution. In contrast, the rate of adsorption declines to 87% because of the increase in AC (50 mg) and lower dye concentration (5 mg/L), possibly caused by the aggregation of AC particles and reduced interaction with dye molecules.

The effect of temperature on CR removal seems notable with CR concentration variation, as depicted in Figure 5c, where the removal of dyes markedly decreases from 94% to 84% with a rise in temperature from 25 to 45 ℃. The exothermic character of the process is responsible for the decline in adsorption with increasing temperature, considering the respective pH of 11. This trend may also be elucidated as an increase in temperatures leading to reduced interactions between the adsorbate and adsorbent, consequently resulting in a decrease in adsorption. Moreover, the observed increase in desorption steps at higher temperatures compared to adsorption suggests a reversible adsorption process [69].

The comparatively minor impact on the removal percentage is apparent in Figure 5d, where both pH and AC dosage result in minimal changes in the CR removal percentage. As discussed earlier, weaker interaction between the prepared AC material and CR at high pH accompanied by the high AC dosage results in 97% of the dye removal. In contrast, at low pH (3) and low AC dose (10 mg), almost 100% of the dye removal was observed. The slight increase in the removal percentage can be attributed to the synergistic impact of the pH level and AC concentration on the removal of the dyes from the bath.

The combined influence of temperature with pH and temperature is illustrated in Figures 5e and 5f, emphasizing the role of temperature, pH, and AC dose in CR dye removal. The cumulative impact of the low pH and temperature in the range of 30-35 ℃ results in the removal of almost all the dyes from the solution. However, the adsorption percentage decreases to 92% due to the rise in temperature (45 ℃) and pH value (11), which could be explained by the weaker contact at

568 higher pH and the exothermic character of the adsorption process. Similarly, at high AC dose
569 and temperature, 93% of the removal was found as compared to low temperature and AC dosage,
570 which resulted in 99% of the removal as per Figure 5f. These results may be explained by the
571 fact that CR demonstrates an exothermic nature at pH 11 (basic condition) while an endothermic
572 nature at a low pH of 3-7.

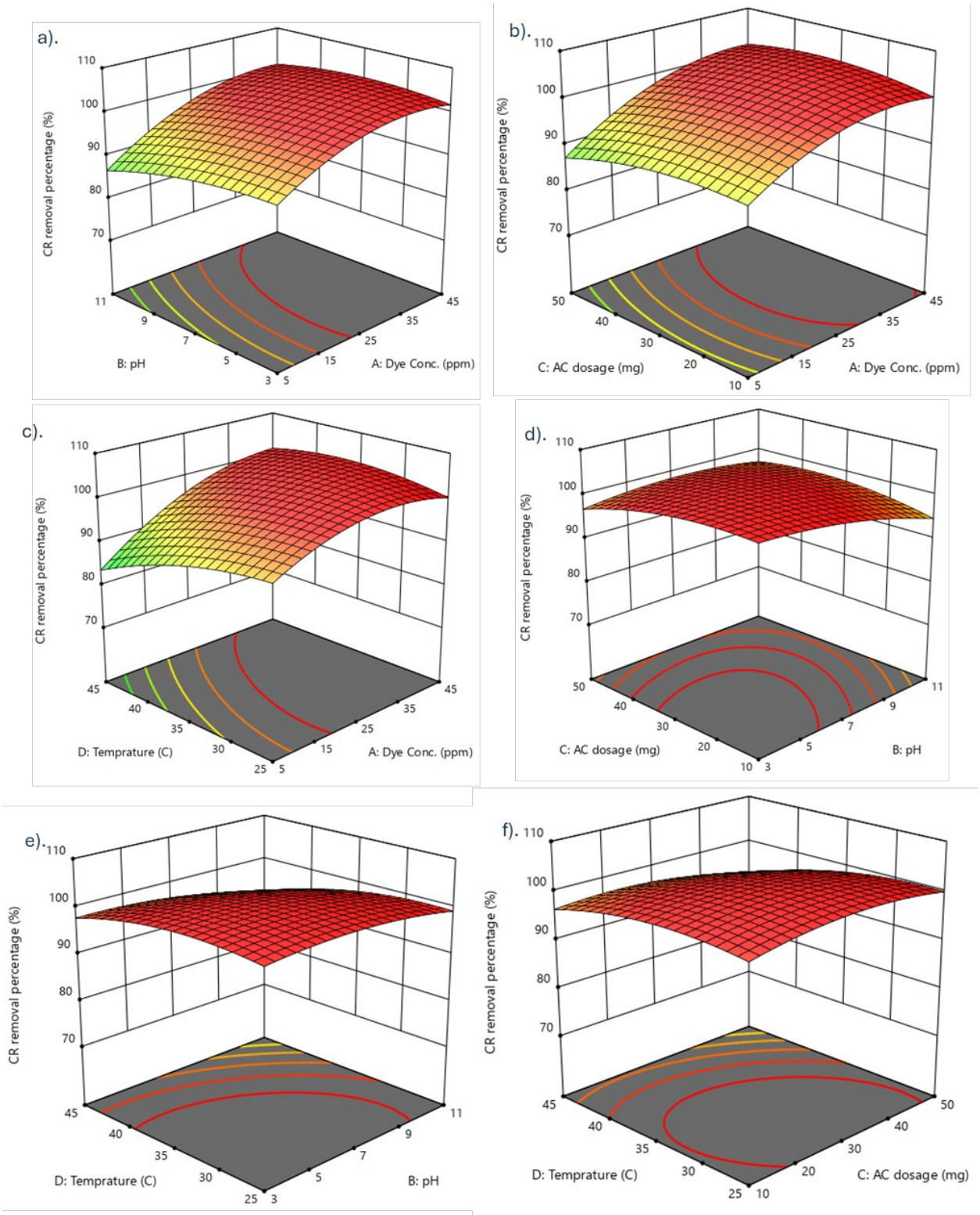

Fig. 5. 3D response surface plot for CR removal as a function of (a) pH versus dye concentration, (b) AC dose versus dye concentration, and (c) Temperature versus dye concentration. (d) AC versus pH (e) Temperature versus pH (f) Temperature versus AC dose.

A diagnostic plot (Figure 6) demonstrates a strong correlation between model predictions and observed values for both dyes, with R^2 values of 0.977 and 0.854 for MB and CR, respectively. The findings indicate that the CCD model offers a reliable evaluation of the investigated adsorption process.

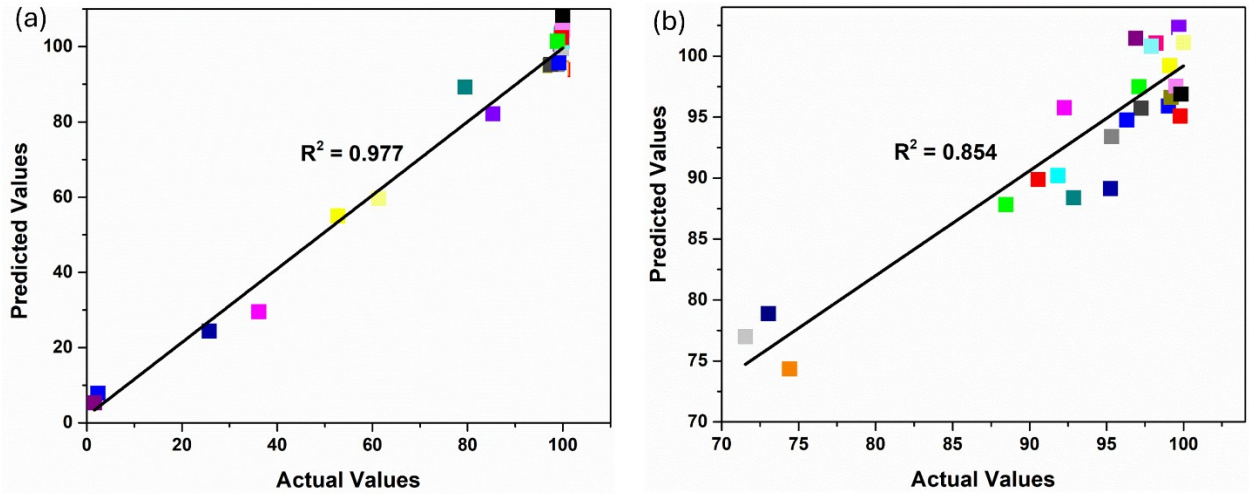

Fig. 6. Predicted vs. experimental data points showing the variance in (a) MB and (b) CR removal.

3.3. Adsorption mechanism

The mechanism of adsorption of dyes on T-AC is controlled by the enhanced surface area to offer optimum adsorption capacity. The elevated surface area allows higher concentrations of dyes to successfully adsorb, allowing optimum removal along with reduction in special sites [70]. The ionizable organic pollutants adsorb with the help of conventional electrostatic forces [71]. MB exists as monomeric MB^+ and dimeric MB_2^+ forms in aqueous solutions, and these cationic species interact with the surface of T-AC through various mechanisms. Electrostatic attraction occurs between the positively charged MB ions and negatively charged sites on T-AC, ensuring strong adsorption under basic conditions having $pH_{solution} > pH_{PZC}$ [72]. The pH of the solution is thus responsible for the deprotonated and negatively charged carboxylate ligands (–COO^-) of the carboxylic groups, which ultimately bind CR and charged MB. The one hydrogen bond donor and one hydrogen bond acceptor for T-AC, along with the acidic functional group, supported the hydrogen bonding for the process by which dyes adhere to the surface [70]. Hydrogen bonding interactions can occur between the surface hydrogens of the hydroxyl groups

(H-donors) present on the surface of T-AC and the nitrogen atoms (H-acceptors) of MB. The FT-IR spectrum of the MB adsorbed sample, as shown in Fig. 3(a), shows a significant decrease in the intensity of –OH groups around 3500 cm^{-1}, along with a slight shift to higher wavenumbers, indicating dipole-dipole bonding interactions. Morphology of T-AC and the van der Waals forces supported the physical adsorption of dyes. Microporosity and activated sites enable abundant adsorption sites for dyes. This interaction is highly dependent on physical parameters, rendering this adsorption a reversible process. The temperature and concentration of dyes are key defining factors for physical adsorption [73]. As shown in Fig. 7, The π–π stacking interactions and electrostatic interactions support the inherent nature of CR to interact with positively charged sites on AC under acidic conditions, enhancing adsorption via ion exchange mechanisms [72]. In this study, oxygen in the carbonyl groups on the adsorbent surface functions as an electron donor, while the aromatic rings with functional groups serve as electron acceptors on MB and CR. The cation exchange occurs when the positively charged MB molecules replace cations, such as hydrogen or metal ions, on the surface of the AC, facilitating strong adsorption. Additionally, complexation arises through interactions between the functional groups on the AC, such as hydroxyl (-OH) or carbonyl (C=O) groups, and the dye molecules, resulting in the formation of coordination bonds. These mechanisms contribute to the enhanced adsorption capacity and stability of the adsorbed dye [74]. Zeta potential analysis is crucial for understanding the surface charge behavior of AC, which significantly influences its interactions with cationic and anionic dyes. As illustrated in Figure S-1 (Supplementary Material), the synthesized AC exhibits a point of zero charge (pH_{ZPC}) at 6.9, indicating a negative surface charge in alkaline conditions that favor MB adsorption and a positive charge in acidic environments that enhance CR removal. These findings align with experimental results in this work and previously reported literature. For instance, Lana S. Maia et al. reported a pH_{ZPC} of approximately 6 for AC derived from palm fibers used for MB removal [75]. Sujata Mandal et al. observed a pH_{ZPC} of 6.2 for kenaf core-based AC applied to CR and heavy metal adsorption [76]. Hatice Karaer Yağmur et al. and Noppon Somsesta et al. documented pH_{ZPC} values of 7 and 6.7 for coconut shell and sisal fiber-based ACs, respectively, both utilized for MB removal [77,78]. Rameez Ahmad Aftab et al. reported a higher pH_{ZPC} of 7.5 for black cardamom-derived AC used in CR adsorption [79]. The literature-derived pH_{ZPC} range of 6-7.5 corroborates with the findings in current research, underscoring the critical role of surface charge in optimizing dye

adsorption through electrostatic interactions.

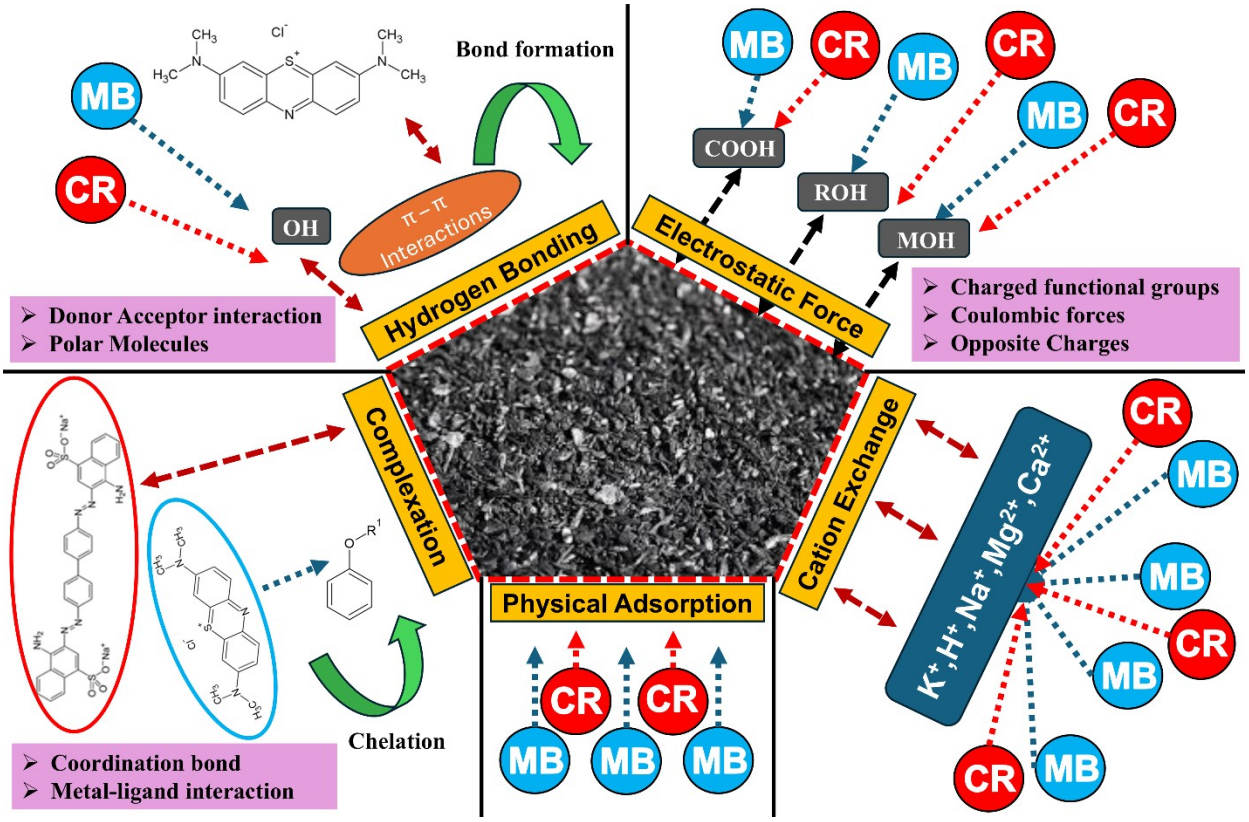

Fig. 7. Possible interaction mechanisms between MB and CR dye with AC.

3.4. Kinetic modelling

Fig. 8 (a-b) shows how contact time affects MB and CR adsorption with AC. When dye molecules engage with easily accessible active sites on the carbon surface, the adsorption process starts quickly. It then slows down as diffusion into the pores takes place until equilibrium is achieved. The number of interaction-ready active sites determines the adsorption rate, which decreases with time. Equilibrium was reached for MB adsorption (pH = 12) in 120 min, with a

maximum adsorption capacity of 16.356 mg/g and removal efficiency of 98.13% (Fig. 8a). An impressive 82.94% efficiency was recorded in the first half hour, suggesting a high rate of adsorption in the early stages. Likewise, CR adsorption (pH = 7) reached an equilibrium in 120 minutes with a 98.91% removal efficiency and 16.486 mg/g adsorption capacity (Fig. 8b). The greater molecular size of CR limits its diffusion through the activated carbon's pores. The CR molecule has -N=N- 2 azo groups and a sulfonic acid group attached to the naphthalene group, making its molecular weight 696.66 g/mol compared to MB, which is 319.85 g/mol consisting of thiazine dye with an aromatic chain that explains why its adsorption is slower but higher in CR than that of MB [52].

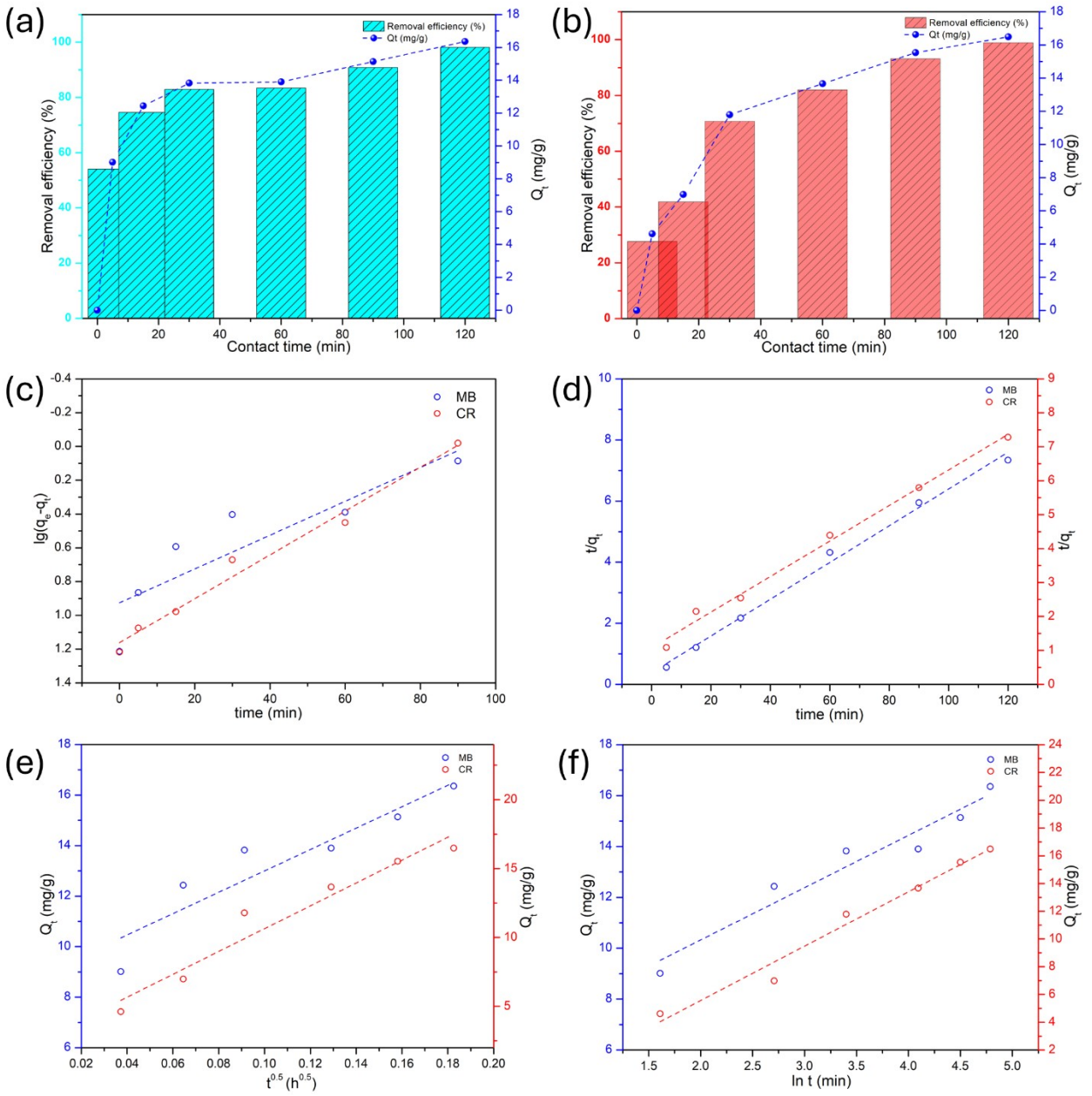

Fig. 8. Contact time of adsorption on AC for (a) MB, (b) CR, and Kinetic models, (c) Pseudo-first-order, (d) Pseudo-second-order, (e) Webber-Morris intraparticle diffusion, and (f) Elovich Model.

The adsorption process was investigated using a variety of kinetic models to determine the mechanism underlying dye removal. Plotting $\ln(q_e - q_t)$ *vs. t* in Fig. 8(c) shows that the pseudo-first-order kinetic model fits both MB and CR. Nevertheless, MB and CR's computed adsorption capacities (q_e) were 8.431 mg/g and 14.504 mg/g, respectively, which differed greatly from their experimental values of 16.356 mg/g and 16.486 mg/g. According to the regression coefficients

(R^2) for MB (0.7816) and CR (0.9824), the pseudo-first-order model fits CR data relatively well but captures the adsorption kinetics for MB poorly. This suggests that the predominant mechanism for MB could not be physical adsorption. The pseudo-second-order model plots *(t/q_t vs. t)* in Fig. 8(d), on the other hand, demonstrate a superior linear fit for both dyes. The data predicted by the model and the experimental data seem to agree quite well, according to the regression coefficients (R^2 = 0.9941 for MB and R^2 = 0.9931 for CR (Table 7)). For MB and CR, the computed adsorption capacities (q_e) of 16.639 mg/g and 19.120 mg/g, respectively, are in good agreement with their experimental values. Given its lower molecular size and easier access to the adsorbent's active sites, MB exhibits a faster adsorption rate, as seen by its higher k_2 value (0.009 g/mg·min) in comparison to CR (0.003 g/mg·min).

Table 7. Kinetic models and their determining parameters related to the removal of MB and CR using AC.

Pseudo-first-order			**Pseudo-second order**		
	MB	CR		MB	CR
$q_{e,}$ *exp (mg/g)*	16.356	16.486	$q_{e,}$ *exp (mg/g)*	16.356	16.486
q_e, *cal (mg/g)*	8.431	14.504	q_e, *cal (mg/g)*	16.639	19.120
K_1 *(min^{-1})*	0.01	0.013	K_2 *(g/mg min)*	0.009	0.003
R^2	0.7816	0.9824	R^2	0.9941	0.9931
SSE	0.173	0.019	*SSE*	0.220	0.194
Intraparticle diffusion			**Elovich**		
K_3 *(mg/g min$^{0.5}$)*	42.328	82.931	α	9.958	0.143
C (mg/g)	8.768	2.348	β	2.057	3.921
R^2	0.867	0.946	R^2	0.944	0.976
SSE	4.303	6.097	*SSE*	1.798	2.764

According to the intraparticle diffusion model Fig. 8(e), adsorption occurs in three stages: (i) a steep slope at the beginning that represents external surface adsorption, (ii) a slower linear region that represents intraparticle diffusion inside the pores, and (iii) a plateau reaching equilibrium [80]. Both dyes exhibit linearity in the q_t *vs.* $t^{0.5}$ plot, however, the lines do not intersect the origin, indicating that there are other rate-limiting mechanisms besides intraparticle diffusion. The high regression values (R^2 = 0.867 for MB and R^2 = 0.976 for CR) show that intraparticle diffusion plays a significant element in the entire adsorption process. The intercept (C) values indicate the boundary layer's thickness, which is 8.768 mg/g for MB and 2.348 mg/g for CR. A greater value for MB indicates a more pronounced film diffusion effect during adsorption. Yeo

Shi Hao et al. have shown similar outcomes in the literature when employing AC derived from waste newspapers as an adsorbent for these dyes [81].

The kinetic results were further corroborated by the Elovich model (Fig. 8(f)), which had regression coefficients of 0.944 for MB and 0.976 for CR. MB was rapidly absorbed at first, as evidenced by the initial adsorption rate (α) being significantly higher for MB (9.958 mg/g·min) than for CR (0.143 mg/g·min). The desorption constant (β) for CR is lower (3.921) than that of MB (2.057), indicating that the molecular size of CR inhibits its ability to penetrate the pores of the adsorbent.

3.5. Isothermal study

The adsorption properties of MB and CR dyes on AC were investigated by analyzing the parameters of the Freundlich and Langmuir models. Figure 9(a-b) presents the linear fitting of the C_e/q_e *vs.* C_e plots based on the Langmuir model. Likewise, Figure 9(c-d) illustrates the linear fitting of the lnq_e *vs.* lnC_e plots following the Freundlich model for the AC samples. A comparison between the Langmuir and Freundlich models revealed that the adsorption of MB satisfied the Langmuir isotherm while the adsorption of CR is favored by both the Langmuir and Freundlich model, as indicated by the linear fitting of the experimental data and R^2 values (Table 8).

The experimental data for MB better fits the Langmuir isotherm model, as evidenced by higher correlation coefficients (R^2=0.998) while low in the case of Freundlich (R^2=0.427). The Langmuir parameters, maximum adsorption capacities (Q_{max}) of 3.33 mg/g for MB and 3.062 mg/g for CR, and Langmuir constants (K_L) of 7.77 for MB and 2.55 for CR were found. Moreover, the R^2 values with regard to the Freundlich model are found to be 0.843 for MB and 0.994 for CR. Thus, the results suggest the monolayer adsorption behavior of MB on the AC surface, while heterogeneous multilayer adsorption sites are present in the case of CR. Although CR's Langmuir parameters indicate some monolayer capacity, the higher R^2 value for the Freundlich model and the lower K_L value suggest that multilayer adsorption on heterogeneous surfaces is more significant for CR, underscoring surface heterogeneity [82]. The structural complexity of CR, including aromatic rings and sulfonate groups, allows it to interact with

various adsorption sites—such as defects, pores, and functional groups like –OH and –COOH on AC [83]. These interactions lead to non-uniform binding energies and multilayer formation. In contrast, MB's smaller size and cationic nature favor monolayer adsorption on homogeneous, high-affinity sites, such as negatively charged AC surfaces, as reflected in its higher Langmuir constant (K_L = 7.77) compared to CR (K_L = 2.55).

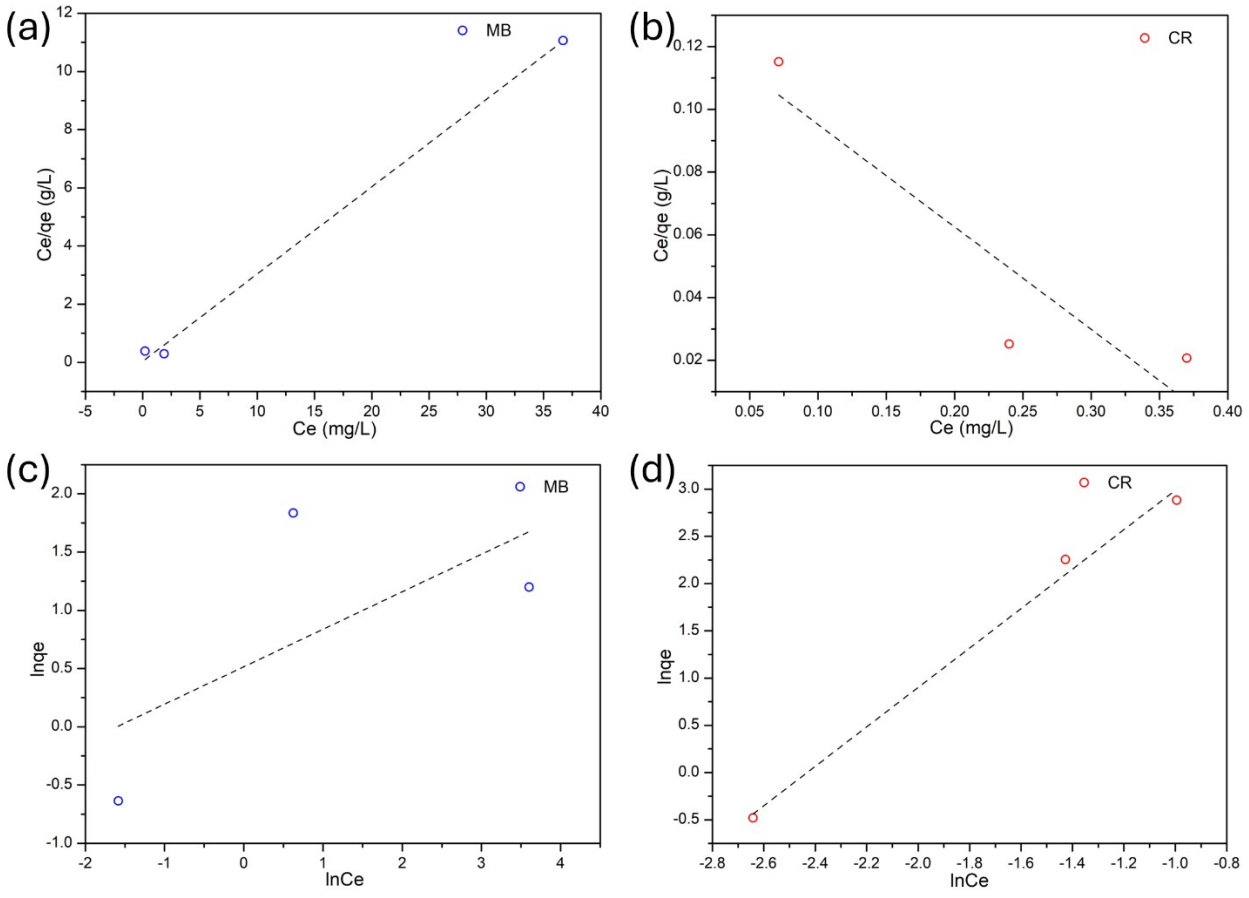

Figure 9. Langmuir adsorption isotherm for (a) MB (b) CR dyes and Freudlich adsorption isotherm for (c) MB (d) CR dyes.

Table 8. Langmuir and Freudlich adsorption isotherm for MB and CR dyes.

Dyes	**Langmuir adsorption isotherm**			**Fruendlich adsoption isotherm**		
	Q_{max} (mg/g)	**K_L**	***R^2***	**n**	**K_F**	***R^2***
MB	3.333	7.772	0.998	3.108	1.675	0.427

CR	3.062	2.556	0.843	0.479	159.780	0.994

3.6. Thermodynamic study

Industrial wastewater effluents are released in water streams at pH 6-8.5; therefore, pH 7 from experimental runs was used to analyze thermodynamics. As predicted by the computed data, Δ*G* was found to be negative for MB, suggesting favorable adsorption and that the reaction was spontaneous. Also, the value of Δ*H* is negative, which clarifies the exothermic nature of MB's adsorption on AC, which is further elaborated by the fact that higher adsorption was favored at low temperatures. The amount of adsorption removal decreased gradually when the temperature was raised from 296 K to 308 K, comparing the experimental runs 16 with 17 (**Table 3**). The highest removal of 99.8% was observed at 308 K at an MB concentration of 25 mg/L, pH 7, and AC dosage of 30 mg. Moreover, Δ*S* being negative suggests that the adsorption of MB is enthalpy-driven. In contrast, the Δ*G* value in the case of CR is likewise negative, indicating that the adsorption process is spontaneous. However, the value of Δ*H* is positive, which confirms the CR adsorption on AC to be endothermic. This is further clarified by the fact that adsorption increases with temperature (see experimental runs 16, 17, and 25 (**Table 5**). At a temperature of 296 K, the adsorption of CR was 98.2%, while at an increased temperature of 308 K, the removal was found to be 99.76%, and at 320 K, the adsorption was 99.79%, with all other parameters kept constant.

Table 9. Thermodynamic parametric values for the adsorption of MB and CR. (Conditions: pH = 7, Conc. = 25 mg/L, and AC dosage = 30 mg)

Parameters		**Temperature**	
for MB	*296 K*	*308 K*	*320 K*
ΔG (kJ/mol)	-15.05	-15.03	-14.99
ΔH (kJ/mol)		-15.72	
ΔS (J/mol K)		-2.24	
Parameters		**Temperature**	
for CR	*296 K*	*308 K*	*320 K*
ΔG (kJ/mol)	-10.59	-13.92	-17.25
ΔH (kJ/mol)		71.57	
ΔS (J/mol K)		277.59	

3.7. Mix Matrix and Reusability Study

Fig. 10(a-b) depicts the reusability performance of AC for the removal of MB and CR dyes over five adsorption cycles. The removal efficiency for MB started at an impressive 98.13% in the first cycle, showcasing the strong affinity of MB molecules for the AC surface. However, this efficiency gradually declined to 27.13% by the fifth cycle. The plausible reason for the observed decrease in adsorption efficiency is the partial loss of AC during the regeneration process. To further investigate the structural and surface chemistry changes in the AC after repeated adsorption-desorption cycles, SEM and FTIR analyses were conducted. The SEM results (Figure S2) revealed no significant differences in surface morphology between the residual AC powder after the 1st and 5th cycles, indicating that the structural integrity and quality of the synthesized AC remained consistent throughout the cycles. Similarly, FTIR analysis (Figure S3) of the samples from the 1st to the 5th cycle showed no notable changes, further confirming the stability of the AC's surface chemistry. These findings demonstrate that the observed slight decrease in efficiency after successive cyclic runs is primarily attributed to the loss of initial dosage quantity during the regeneration process rather than any structural or chemical degradation of the AC. The relatively high efficiency during the early cycles suggests that MB adsorption is governed primarily by weaker interactions, such as electrostatic forces and hydrogen bonding, which are partially reversible [84,85]. However, for CR, the removal efficiency followed a similar downward trend but with a much sharper decline, decreasing from 98.25% in the first cycle to 12.09% by the fifth cycle. The steeper drop in performance can be attributed to the larger molecular size and more complex structure of CR, which introduces significant steric hindrance and stronger interactions with the AC surface. These factors make desorption more challenging and limit the availability of active sites for subsequent cycles. The observed trends are strongly influenced by the molecular properties of MB and CR. MB, being a cationic dye with a smaller molecular size, exhibits easier adsorption and partial regeneration, maintaining moderate efficiency over several cycles. Conversely, CR, as an anionic dye with a larger and more complex molecular structure, forms stronger and more irreversible bonds with the AC surface, resulting in a faster saturation for removal efficiency [86].

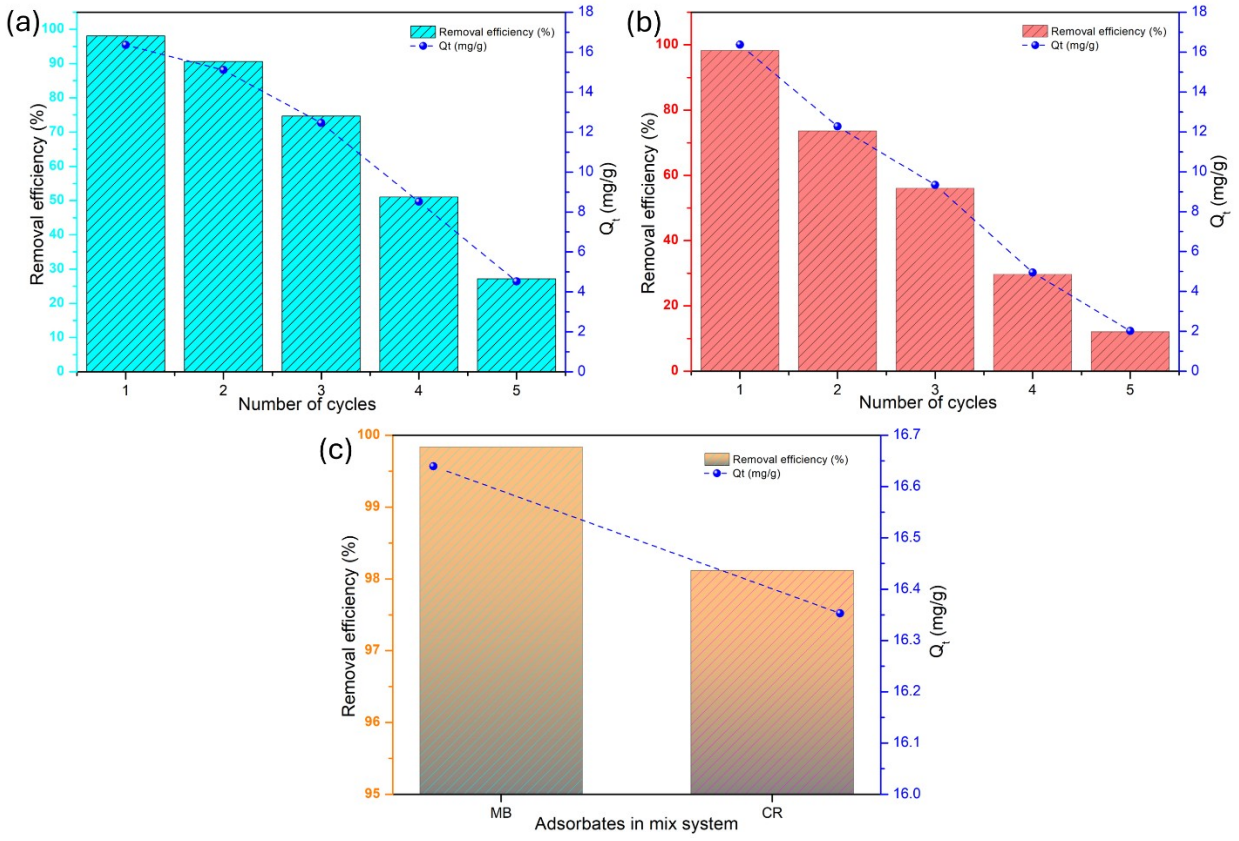

Figure 10. (a) Reusability of Mb, (b) Reusability of CR, and (c) interaction of MB and CR in a mixed matrix.

The removal effectiveness and adsorption capacity of MB and CR dyes in a mixed dye system under two ideal circumstances are contrasted in Fig. 10c (pH 12 for MB and pH 7 for CR). The MB dye exhibits dominant adsorption capability at pH 12 and 665 nm wavelength with a capacity of 0.188 mg/g and a removal efficiency of around 100%. On the other hand, CR shows superior adsorption efficacy at pH 7 and 498 nm, having a marginally lower removal effectiveness of about 97% and an adsorption capacity of 0.184 mg/g. The results suggest the optimal removal of the two dyes in a mixed matrix at their respective pH values, as evident from the RSM modeling.

3.8. Comparative study with other adsorbents

Table 10 below shows the removal of MB and CR via the adsorption process using different absorbents. The adsorption performance was compared using surface area and adsorption capacity at optimum conditions. As can be seen, the AC derived from waste polyester matrix was

able to completely remove MB and 99% of CR with an adsorption capacity of 89 mg/g for both owing to its surface area of 167.08 m^2/g, which is relatively high in contrast to other recently reported materials in the literature for removing MB and CR dyes. Thus, the adsorbent reported in this study can potentially be used as an effective material for the removal of dyes.

Table 10. Comparative removal of MB and CR by adsorbents in literature.

Methylene Blue				
Adsorbents	**Surface area (m^2/g)**	**Optimum conditions**	**Adsorption capacity (mg/g)**	**Reference**
Oil palm (EFB)	35.6328	pH= 2, Conc.= 50 mg/L, dosage= 5 g/L	8.26	[87]
nano-iron loaded mesoporous silica	29	pH= 7, Conc.= 5 mg/L, dosage= 10 mg	14.78	[88]
coffee husk AC	0.9853	pH= 8.12, Conc.= 100 mg/L, dosage= 5 g/L	88.1	[89]
Tectona Grandis	1.058	pH= 7, Conc.= 100 mg/L, dosage= 10 mg	35.7	[90]
Polyester matrix-derived AC	**167.08**	pH= 11, Conc.= 45 mg/L, dosage= 10 mg	**89**	**This Study**
Congo Red				
Adsorbents	**Surface area (m^2/g)**	**Optimum conditions**	**Adsorption capacity (mg/g)**	**Reference**
Ag–Cu–CeO_2 nanocomposites	78.361	pH= 2, Conc.= 55.6 mg/L, dosage= 100 mg	4.71	[91]
Black cardamom	196	pH=6, Conc.= 100 mg/L, dosage= 100 mg	69.9	[79]
Hemp Hurd Biochar	17.64	pH= 8, Conc.= 10 mg/L, dosage= 600 mg	15.34	[92]
Cu/Al-LDHs@Gltn	41.35	pH=2, Conc.= 15 mg/L, dosage= 15 mg	15.85	[93]
Polyester matrix-derived AC	**167.08**	pH= 3, Conc.= 45 mg/L, dosage= 10 mg	**89**	**This Study**

4. Conclusions

In this study, a sustainable and efficient method was developed to create AC from polyester waste using a $ZnCl_2$-assisted chemical activation process. The resultant AC demonstrated exceptional efficacy in eliminating MB and CR dyes from water. To attain the highest dye removal effectiveness, RSM was used to assess the optimized critical parameters, including pH, temperature, adsorbent dosage, and dye concentration. The AC's high adsorption capacity was attributed to the strong interaction between its oxygen-containing functional groups (–OH and –COOH) and the dye molecules. The zeta potential revealed pH_{ZPC} at 6.9 for AC, indicating a negative surface charge in alkaline conditions that favor MB adsorption and a positive charge in acidic environments for enhanced CR removal. Under optimal conditions—pH 11 for MB and pH 7 for CR, an adsorbent dosage of 30 mg, a dye concentration of 25 mg/L, and a temperature of 35 ℃—the removal efficiency reached 100% for MB and 99% for CR. According to kinetic investigations, the adsorption mechanism adhered to intra-particle diffusion and pseudo-second-order models, confirming chemisorption as the primary mechanism. Furthermore, MB satisfied the Langmuir isotherm, while the adsorption of CR was favored by both the Langmuir and Freundlich models owing to its structural complexity, including aromatic rings and sulfonate groups, which allows it to interact with various adsorption sites—such as defects, pores, and functional groups of AC. The thermodynamic analysis showed that MB adsorption was exothermic, while CR adsorption was endothermic. Reusability tests further highlighted the reusability of the AC, maintaining its high adsorption efficiency over multiple cyclic runs with no significant structural changes. This research showcases the potential of converting polyester waste into a high-performance AC for dye removal. It offers a cost-effective and eco-friendly approach to addressing wastewater treatment challenges. This study was batch testing, and future studies would focus on immobilizing the AC to a functionalized membrane that can be tested in a continuous flow mode along with the effect of competing ions to determine practical applicability at a pilot scale to counter wastewater treatment over a large scale.

Acknowledgments

The authors are thankful to the Higher Education Commission (HEC) Government of Pakistan for funding this study under the NRPU program through Project No. 15188. We are thankful to Fiber Craft Industries (FCI) in Lahore, Pakistan, for supplying composite waste material. The

authors (M.Y and V.S) gratefully acknowledge the support from the European Just Transition Fund within the Operational Programme: Just Transition under the aegis of the Ministry of the Environment of the Czech Republic, project CirkArena number CZ.10.03.01/00/22_003/0000045 and the Ministry of Education Youth and Sports of the Czech Republic, Operational Programme Johannes Amos Comenius OP JAC "Application potential development in the field of polymer materials in the context of circular economy compliance (POCEK)", number CZ.02.01.01/00/23_021/0009004. The authors are further grateful for co-funding from the development process of the Centre of Polymer Systems, Tomas Bata University in Zlin, program DKRVO (RP/CPS/2024-28/002) supported by the Ministry of Education Youth and Sports of the Czech Republic. M.Y also expresses his gratitude for support within the “Creativity, Intelligence & Talent for the Zlin Region” (CIT - ZK) program.

Conflict of interest

The authors declare no competing financial interests or personal connections that would influence the reported study.

Credit authorship contribution statement

Farhan Raheel Asif: Conceptualization, Methodology, Investigation, Formal analysis, Data curation, Writing- original draft, Writing- review & editing.

Bushra Bibi: Experimentation, methodology, investigation, validation.

Muhammad Yasir: Conceptualization, Formal analysis, Data curation, Writing- review & editing.

Imran Ahmad Khan: Formal analysis, Data curation

Jawad Gul: Methodology, Writing- original draft.

Sofia Javed: Data curation, supervision, resources.

Vladimir Sedlarik: Project administration, Funding acquisition.

Muhammad Irfan: Conceptualization, Supervision, Project administration, Funding acquisition, Review & editing.

References

[1] K. Formela,, M. Kurańska,, M. Barczewski, Polymers (Basel). (2022).

10.3390/polym14051050.

[2] I.O. Oladele,, A.A. Adediran,, A.D. Akinwekomi,, M.H. Adegun,, O.O. Olumakinde,, O.O. Daramola, Sci. World J. 2020 (2020). 10.1155/2020/7462758.

[3] K. Pender,, L. Yang, Polym. Compos. 40(9) (2019) 3510–9. https://doi.org/10.1002/pc.25213.

[4] Y. Tao,, S.A. Hadigheh,, Y. Wei, Structures 53 (2023) 1540–56. https://doi.org/10.1016/j.istruc.2023.05.018.

[5] X. Yang,, H. Tang,, Y. Li,, Y. Zhan,, Y. Li,, F. Zhong,, P. Wang,, W. Feng,, K. Li, Polym. Degrad. Stab. 224 (2024) 110754. https://doi.org/10.1016/j.polymdegradstab.2024.110754.

[6] A. Rafay,, M. Irfan,, S.R. Naqvi,, M.A. Umer,, M.A. Rehman,, M. Saleem,, M.S. Butt,, A.U. Khan, Polym. Compos. 45(18) (2024) 16616–29. https://doi.org/10.1002/pc.28916.

[7] A. Sahu,, J.C. Poler, J. Environ. Chem. Eng. 12(5) (2024) 113754. https://doi.org/10.1016/j.jece.2024.113754.

[8] Z.M. Şenol,, H. Arslanoğlu,, Z.S. Keskin,, V. Mehmeti,, N. El Messaoudi, Int. J. Biol. Macromol. 298 (2025) 139264. https://doi.org/10.1016/j.ijbiomac.2024.139264.

[9] T. Aravinda,, K. Kavya,, G. Nagendra,, M. Srinivas,, P. Vishwa,, S. Kandaiah,, A. Nizam,, K. Munirathnam,, K.B. Ramesh, Mater. Sci. Eng. B 296 (2023) 116633. https://doi.org/10.1016/j.mseb.2023.116633.

[10] M. Bin Mobarak,, N.S. Pinky,, F. Chowdhury,, M.S. Hossain,, M. Mahmud,, M.S. Quddus,, S.A. Jahan,, S. Ahmed, J. Saudi Chem. Soc. 27(5) (2023) 101690. https://doi.org/10.1016/j.jscs.2023.101690.

[11] S. Ijaz,, A. Kausar,, M. Iqbal,, N. El Messaoudi,, Y. Miyah,, S. Knani,, B. Graba, J. Water Process Eng. 71 (2025) 107187. https://doi.org/10.1016/j.jwpe.2025.107187.

[12] D. Bhatia,, N.R. Sharma,, J. Singh,, R.S. Kanwar, Crit. Rev. Environ. Sci. Technol. 47(19)

(2017) 1836–76. 10.1080/10643389.2017.1393263.

[13] N. El Messaoudi,, Y. Miyah,, N. Singh,, S. Gubernat,, R. Fatima,, J. Georgin,, A. El Mouden,, S. Saghir,, S. Knani,, Y. Hwang, J. Environ. Chem. Eng. 12(6) (2024) 114843. https://doi.org/10.1016/j.jece.2024.114843.

[14] Holilah,, Asranudin,, N. El Messaoudi,, M. Ulfa,, A. Hamzah,, Z.A.A. Hamid,, D.V. Ramadhani,, L. Suryanegara,, M. Mahardika,, A.T. Melenia,, A.W. Pratama,, D. Prasetyoko, Case Stud. Chem. Environ. Eng. 10 (2024) 100850. https://doi.org/10.1016/j.cscee.2024.100850.

[15] P.O. Oladoye,, T.O. Ajiboye,, E.O. Omotola,, O.J. Oyewola, Results Eng. 16 (2022) 100678. https://doi.org/10.1016/j.rineng.2022.100678.

[16] P.M. Thabede,, N.D. Shooto,, E.B. Naidoo, South African J. Chem. Eng. 33 (2020) 39–50. https://doi.org/10.1016/j.sajce.2020.04.002.

[17] P.O. Oladoye,, M.O. Bamigboye,, O.D. Ogunbiyi,, M.T. Akano, Groundw. Sustain. Dev. 19 (2022) 100844. https://doi.org/10.1016/j.gsd.2022.100844.

[18] T.E. Rasilingwani,, J.R. Gumbo,, V. Masindi,, S. Foteinis, Water Resour. Ind. 31 (2024) 100253. https://doi.org/10.1016/j.wri.2024.100253.

[19] Z. Ciğeroğlu,, N. El Messaoudi,, Y. Miyah,, J. Georgin,, D.S.P. Franco,, M. Benjelloun,, Z.M. Şenol,, E.S. Kazan-Kaya,, B. Temur Ergan, Sustain. Mater. Technol. 42 (2024) e01187. https://doi.org/10.1016/j.susmat.2024.e01187.

[20] Y. Miyah,, M. Benjelloun,, F. Mejbar,, S. Ssouni,, M. El-Habacha,, S. Iaich,, N. El Messaoudi,, M. Zerrouq,, M. Souilah,, A. Lahrichi,, F. Zerrouq, Results Chem. 13 (2025) 102038. https://doi.org/10.1016/j.rechem.2025.102038.

[21] A.A. Alqadami,, S.M. Wabaidur,, B.-H. Jeon,, M.A. Khan, Biomass Convers. Biorefinery 14(14) (2024) 15757–68. 10.1007/s13399-022-03711-7.

[22] M. Azam,, S.M. Wabaidur,, M.R. Khan,, S.I. Al-Resayes,, M.S. Islam, Polymers (Basel).

(2022). 10.3390/polym14050914.

[23] E. Kurtulbaş,, Z. Ciğeroğlu,, S. Şahin,, N. El Messaoudi,, V. Mehmeti, Int. J. Biol. Macromol. 274 (2024) 133378. https://doi.org/10.1016/j.ijbiomac.2024.133378.

[24] E. Robens, in: J. Rouquerol, F. Rodríguez-Reinoso, K. S. W. Sing, K. K. B. T.-S. in S. S. and C. Unger (Eds.), Characterization of Porous Solids III, Vol. 87, Elsevier, 1994, pp. 109–18.

[25] Y. Miyah,, N. El Messaoudi,, M. Benjelloun,, J. Georgin,, D.S.P. Franco,, Y. Acikbas,, H.S. Kusuma,, M. Sillanpää, Mater. Today Sustain. 28 (2024) 100985. https://doi.org/10.1016/j.mtsust.2024.100985.

[26] B. Tekin,, Y. Topcu, J. Energy Storage 77 (2024) 109879. https://doi.org/10.1016/j.est.2023.109879.

[27] M. Atay,, D. Duran Kaya,, A. Ülker, Polymers (Basel). (2023). 10.3390/polym15224469.

[28] I.A. Khan,, A.U. Khan,, K.M. Deen,, E. Asselin,, R. Sadiq,, M. Yasir,, N. Ahmad, Mater. Res. Express (2024). 10.1088/2053-1591/ad76fe.

[29] H. Kim,, S.H. So,, R. Muhammad,, H. Oh, Int. J. Hydrogen Energy 50 (2024) 1616–25. https://doi.org/10.1016/j.ijhydene.2023.10.160.

[30] I.A. Khan,, K.M. Deen,, E. Asselin,, M. Yasir,, R. Sadiq,, N.M. Ahmad, J. Ind. Eng. Chem. (September) (2024). 10.1016/j.jiec.2024.10.067.

[31] Z. Li,, H. Wu,, D. Zhang,, Q. Wang,, H. Sun,, Q. Sun,, B. Wang, Appl. Surf. Sci. 657 (2024) 159744. https://doi.org/10.1016/j.apsusc.2024.159744.

[32] Y. Li,, Y. Lin,, J. Guo,, Z. Xu,, B. Wang,, T. Zhu, Environ. Sci. Pollut. Res. 29(18) (2022) 26599–612. 10.1007/s11356-021-17724-8.

[33] C.-J. Zheng,, R.-C. Zhang,, K. Xu,, J. Zhang,, K. Wang,, W. Chen,, G.-B. Huang,, H. Yin, Carbon N. Y. 226 (2024) 119153. https://doi.org/10.1016/j.carbon.2024.119153.

[34] N. El Messaoudi,, Y. Miyah,, J. Georgin,, G. Huerta-Angeles,, K. Ansari,, H.A. Said,, F.K. Algethami,, P. Kaur,, L.B.T.-A. in C.P. Meili Environmental Management and Protection, Elsevier, 2024, p. .

[35] L. Zhang,, S. Zuo, Molecules (2024). 10.3390/molecules29133197.

[36] J. Rashid,, F. Tehreem,, A. Rehman,, R. Kumar, Sci. Total Environ. 671 (2019) 369–76. https://doi.org/10.1016/j.scitotenv.2019.03.363.

[37] A. Ibrahim,, A. Ismail,, H. Juahir,, Y.N. Ihsan,, S. Sudianto,, M. Ovinis,, A.M. Kassim,, N.H.M. Hanapi,, A.D. Hafizi, Carbon Trends 13 (2023) 100301. https://doi.org/10.1016/j.cartre.2023.100301.

[38] X. Yu,, S. Wang,, J. Zhang, J. Mater. Sci. 53(7) (2018) 5458–66. 10.1007/s10853-017-1928-2.

[39] Z. Xu,, D. Zhang,, Z. Yuan,, W. Chen,, T. Zhang,, D. Tian,, H. Deng, Environ. Sci. Pollut. Res. 24(28) (2017) 22602–12. 10.1007/s11356-017-9939-8.

[40] L. Feng,, B. Yan,, C. Wang,, Q. Zhang,, S. Jiang,, S. He, in: A. Uthaman, S. Thomas, T. Li, H. Maria (Eds.),Springer International Publishing, Cham, 2022, pp. 587–612.

[41] B. Li,, C. Li,, D. Li,, L. Zhang,, S. Zhang,, Z. Cui,, D. Wang,, Y. Tang,, X. Hu, Fuel Process. Technol. 252 (2023) 107987. https://doi.org/10.1016/j.fuproc.2023.107987.

[42] S. Wei,, Q. Qin,, Z. Liu, J. Anal. Appl. Pyrolysis 179 (2024) 106500. https://doi.org/10.1016/j.jaap.2024.106500.

[43] J. Hu,, D. Shen,, S. Wu,, R. Xiao, J. Anal. Appl. Pyrolysis 127 (2017) 444–50. https://doi.org/10.1016/j.jaap.2017.07.005.

[44] G. Huang,, P. Bian,, X. Wang, Fullerenes, Nanotub. Carbon Nanostructures 32(11) (2024) 993–1004. 10.1080/1536383X.2024.2356235.

[45] G. Wang,, P. Tan,, Z. Kong,, J. Ao,, R. Wang,, Z. Zhang,, Z. Hao, RSC Adv. 14(50) (2024) 37359–69. 10.1039/D4RA07004F.

[46] V. Pimpan,, K. Ruangput,, S. Saenkhot, Mater. Sci. Forum 1064 (2022) 47–52. 10.4028/p-r8ddt9.

[47] H. Zhao,, H. Zhong,, Y. Jiang,, H. Li,, P. Tang,, D. Li,, Y. Feng, Materials (Basel). (2022). 10.3390/ma15030895.

[48] R. Ahmad,, K. Ansari, Process Biochem. 108 (2021) 90–102. https://doi.org/10.1016/j.procbio.2021.05.013.

[49] C. Waghmare,, S. Ghodmare,, K. Ansari,, M.H. Dehghani,, M. Amir Khan,, M.A. Hasan,, S. Islam,, N.A. Khan,, S. Zahmatkesh, J. Environ. Manage. 345 (2023) 118815. https://doi.org/10.1016/j.jenvman.2023.118815.

[50] A.N. Fahanwi,, M. Yasir,, H.T. Nguyen,, N. Saha,, T. Saha,, V. Sedlařík,, P. Saha, Chem. Eng. Res. Des. 201 (2024) 18–30. https://doi.org/10.1016/j.cherd.2023.11.043.

[51] M. Yasir,, F. Asabuwa Ngwabebhoh,, T. Šopík,, L. Lovecká,, D. Kimmer,, V. Sedlařík, J. Chem. Technol. Biotechnol. 97(12) (2022) 3317–32. 10.1002/jctb.7191.

[52] H.-Y. Zhu,, Y.-Q. Fu,, R. Jiang,, J.-H. Jiang,, L. Xiao,, G.-M. Zeng,, S.-L. Zhao,, Y. Wang, Chem. Eng. J. 173(2) (2011) 494–502. https://doi.org/10.1016/j.cej.2011.08.020.

[53] F. Amran,, M.A.A. Zaini, Environ. Technol. Innov. 23 (2021) 101727. https://doi.org/10.1016/j.eti.2021.101727.

[54] A. Moges,, T.T.I. Nkambule,, J. Fito, J. Environ. Manage. 305 (2022) 114369. https://doi.org/10.1016/j.jenvman.2021.114369.

[55] H.M. El-Bery,, M.R. Salah,, S.M. Ahmed,, S.A. Soliman, RSC Adv. 11(22) (2021) 13229–44. 10.1039/D1RA01218E.

[56] A.H. Mahmoud,, H.M. El-Bery,, M.M. Ali,, E.S. Aldaby,, A.M.M. Mawad,, A.A. Shoreit, Biomass Convers. Biorefinery 13(6) (2023) 4785–95. 10.1007/s13399-021-01479-w.

[57] R.A. Canales-Flores,, F. Prieto-García, Diam. Relat. Mater. 109 (2020) 108027. https://doi.org/10.1016/j.diamond.2020.108027.

[58] H.B. Motejadded Emrooz,, M. Maleki,, A. Rashidi,, M. Shokouhimehr, Biomass Convers. Biorefinery 11(3) (2021) 943–54. 10.1007/s13399-019-00584-1.

[59] C.H.K. Lam,, A.W.M. Ip,, J.P. Barford,, G. McKay, Sustainability (2010) 1943–68. 10.3390/su2071943.

[60] A. Sarı,, M. Tuzen, J. Hazard. Mater. 171(1) (2009) 973–9. https://doi.org/10.1016/j.jhazmat.2009.06.101.

[61] Z. Eren,, F.N. Acar, Desalination 194(1) (2006) 1–10. https://doi.org/10.1016/j.desal.2005.10.022.

[62] S. Cheng,, L. Zhang,, H. Xia,, J. Peng,, J. Shu,, C. Li,, X. Jiang,, Q. Zhang, RSC Adv. 7(44) (2017) 27331–41. 10.1039/C7RA01482A.

[63] S. Karaca,, A. Gürses,, M. Açıkyıldız,, M. Ejder (Korucu), Microporous Mesoporous Mater. 115(3) (2008) 376–82. https://doi.org/10.1016/j.micromeso.2008.02.008.

[64] R.S. Alwi,, R. Gopinathan,, A. Bhowal,, C. Garlapati, Molecules 25(24) (2020). 10.3390/MOLECULES25246014.

[65] S. Banerjee,, M.C. Chattopadhyaya, Arab. J. Chem. 10 (2017) S1629–38. https://doi.org/10.1016/j.arabjc.2013.06.005.

[66] M.H. Dehghani,, M. Salari,, R.R. Karri,, F. Hamidi,, R. Bahadori, Sci. Rep. 11(1) (2021) 11613. 10.1038/s41598-021-90914-z.

[67] R. Ahmad,, J. Guo,, J. Kim, J. Clean. Prod. 232 (2019) 608–16. https://doi.org/10.1016/j.jclepro.2019.05.244.

[68] S.T. Akar,, A.S. Özcan,, T. Akar,, A. Özcan,, Z. Kaynak, Desalination 249(2) (2009) 757–61. https://doi.org/10.1016/j.desal.2008.09.012.

[69] M.J. Iqbal,, M.N. Ashiq, J. Hazard. Mater. 139(1) (2007) 57–66. 10.1016/j.jhazmat.2006.06.007.

[70] B.N. Bhadra,, I. Ahmed,, S. Kim,, S.H. Jhung, Chem. Eng. J. 314 (2017) 50–8. https://doi.org/10.1016/j.cej.2016.12.127.

[71] S. Liu,, W. Xu,, Y. Liu,, X. Tan,, G. Zeng,, X. Li,, J. Liang,, Z. Zhou,, Z. Yan,, X. Cai, Sci. Total Environ. 592 (2017) 546–53. https://doi.org/10.1016/j.scitotenv.2017.03.087.

[72] Y. Achour,, L. Bahsis,, E.-H. Ablouh,, H. Yazid,, M.R. Laamari,, M. El Haddad, Surfaces and Interfaces 23 (2021) 100977. https://doi.org/10.1016/j.surfin.2021.100977.

[73] I. Salahshoori,, Q. Wang,, M.A.L. Nobre,, A.H. Mohammadi,, E.A. Dawi,, H.A. Khonakdar, Adv. Colloid Interface Sci. 333 (2024) 103281. https://doi.org/10.1016/j.cis.2024.103281.

[74] X. Fan,, S. Wang,, Y. Zhang,, M. Zhao,, N. Zhou,, S. Fan, Environ. Monit. Assess. 196(7) (2024) 664. 10.1007/s10661-024-12836-3.

[75] L.S. Maia,, A.I.C. da Silva,, E.S. Carneiro,, F.M. Monticelli,, F.R. Pinhati,, D.R. Mulinari, J. Polym. Environ. 29(4) (2021) 1162–75. 10.1007/s10924-020-01951-0.

[76] S. Mandal,, J. Calderon,, S.B. Marpu,, M.A. Omary,, S.Q. Shi, J. Contam. Hydrol. 243 (2021) 103869. https://doi.org/10.1016/j.jconhyd.2021.103869.

[77] H.K. Yağmur,, İ. Kaya, J. Mol. Struct. 1232 (2021) 130071. https://doi.org/10.1016/j.molstruc.2021.130071.

[78] N. Somsesta,, V. Sricharoenchaikul,, D. Aht-Ong, Mater. Chem. Phys. 240 (2020) 122221. https://doi.org/10.1016/j.matchemphys.2019.122221.

[79] R. Ahmad Aftab,, S. Zaidi,, A. Aslam Parwaz Khan,, M. Arish Usman,, A.Y. Khan,, M. Tariq Saeed Chani,, A.M. Asiri, Alexandria Eng. J. 71 (2023) 355–69. https://doi.org/10.1016/j.aej.2023.03.055.

[80] P. Zhou,, X. Li,, J. Zhou,, Z. Peng,, L. Shen,, W. Li, J. Environ. Chem. Eng. 11(5) (2023) 110496. https://doi.org/10.1016/j.jece.2023.110496.

[81] Y.S. Hao,, N. Othman,, M.A.A. Zaini, Int. J. Biol. Macromol. 277 (2024) 134353.

https://doi.org/10.1016/j.ijbiomac.2024.134353.

[82] K.-T. Chan,, S.-T. Ong,, S.-T. Ha, Desalin. Water Treat. 317 (2024) 100060. https://doi.org/10.1016/j.dwt.2024.100060.

[83] D. Sibera,, I. Pełech,, P. Staciwa,, R. Pełech,, E. Ekiert,, G.Y. Kayalar,, U. Narkiewicz, Molecules (2024). 10.3390/molecules29174090.

[84] F.E. Yaacoubi,, C. Sekkouri,, K. Ennaciri,, I. Rabichi,, Z. Izghri,, A. Baçaoui,, A. Yaacoubi, Int. J. Biol. Macromol. 254 (2024) 127706. https://doi.org/10.1016/j.ijbiomac.2023.127706.

[85] T. Somsiripan,, C. Sangwichien, Arab. J. Chem. 16(12) (2023) 105270. https://doi.org/10.1016/j.arabjc.2023.105270.

[86] P.K. Rose,, V. Poonia,, R. Kumar,, N. Kataria,, P. Sharma,, J. Lamba,, P. Bhattacharya, Groundw. Sustain. Dev. 23 (2023) 101005. https://doi.org/10.1016/j.gsd.2023.101005.

[87] L. Baloo,, M.H. Isa,, N. Bin Sapari,, A.H. Jagaba,, L.J. Wei,, S. Yavari,, R. Razali,, R. Vasu, Alexandria Eng. J. 60(6) (2021) 5611–29. https://doi.org/10.1016/j.aej.2021.04.044.

[88] W.M. Saod,, I.W. Oliver,, A. Contini,, V. Zholobenko, J. Mol. Struct. 1319 (2025) 139390. https://doi.org/10.1016/j.molstruc.2024.139390.

[89] P. Deivasigamani,, P. Senthil Kumar,, S. Sundaraman,, M.R. Soosai,, A.A. Renita,, K. M,, N. Bektenov,, O. Baigenzhenov,, V. D,, A. Kumar J, Environ. Res. 236 (2023) 116735. https://doi.org/10.1016/j.envres.2023.116735.

[90] D.N. Shetty,, V.A. Lobo,, S. Rani,, N. Raghavendra, Hybrid Adv. 7 (2024) 100316. https://doi.org/10.1016/j.hybadv.2024.100316.

[91] N. Semwal,, D. Mahar,, M. Chatti,, A. Dandapat,, M. Chandra Arya, Heliyon 9(11) (2023). 10.1016/j.heliyon.2023.e22027.

[92] R.V. Srinadh,, N. Remya, Chem. Eng. Res. Des. 212 (2024) 321–31. https://doi.org/10.1016/j.cherd.2024.11.011.

[93] G.M. Nabil,, R.H. Althomali,, M.E. Mahmoud, J. Mol. Struct. 1319 (2025) 139303. https://doi.org/10.1016/j.molstruc.2024.139303.